Received: September 28, 2022 Revised: April 2, 2023 Accepted: April 24, 2023

https://doi.org/10.1016/j.neurom.2023.04.471

# Biophysical Principles and Computational Modeling of Deep Brain Stimulation

Patrick R. Ng, BS, BA[1]; Alan Bush, PhD[1,2]; Matteo Vissani, PhD[1,2]; Cameron C. McIntyre, PhD[3,4]; Robert Mark Richardson, MD, PhD[1,2]

## ABSTRACT

**Background:** Deep brain stimulation (DBS) has revolutionized the treatment of neurological disorders, yet the mechanisms of DBS are still under investigation. Computational models are important in silico tools for elucidating these underlying principles and potentially for personalizing DBS therapy to individual patients. The basic principles underlying neurostimulation computational models, however, are not well known in the clinical neuromodulation community.

**Objective:** In this study, we present a tutorial on the derivation of computational models of DBS and outline the biophysical contributions of electrodes, stimulation parameters, and tissue substrates to the effects of DBS.

**Results:** Given that many aspects of DBS are difficult to characterize experimentally, computational models have played an important role in understanding how material, size, shape, and contact segmentation influence device biocompatibility, energy efficiency, the spatial spread of the electric field, and the specificity of neural activation. Neural activation is dictated by stimulation parameters including frequency, current vs voltage control, amplitude, pulse width, polarity configurations, and waveform. These parameters also affect the potential for tissue damage, energy efficiency, the spatial spread of the electric field, and the specificity of neural activation. Activation of the neural substrate also is influenced by the encapsulation layer surrounding the electrode, the conductivity of the surrounding tissue, and the size and orientation of white matter fibers. These properties modulate the effects of the electric field and determine the ultimate therapeutic response.

**Conclusion:** This article describes biophysical principles that are useful for understanding the mechanisms of neurostimulation.

**Keywords:** Biophysics, computational modeling, deep brain stimulation

## INTRODUCTION

Deep brain stimulation (DBS) has revolutionized the treatment of intractable neurologic disorders. Despite robust evidence that DBS can be safe and effective, the exact biophysical mechanisms are still under investigation. Stimulation settings are typically titrated on a trial-and-error basis. Side effects emerge from stimulation of off-target sites, and even lead deviations of a few millimeters can dramatically affect clinical benefits.[1]

Computational modeling offers a unique approach to understanding the mechanisms of DBS and may eventually facilitate precision programming in place of traditional trial-and-error approaches. The benefits of computational modeling arise from the potential to study multiple variables, such as stimulation parameters and electrode characteristics, in ways that are difficult to achieve empirically. Studies have shown that computational modeling, when paired with advances in hardware and imaging, can personalize DBS for a patient's specific neuroanatomy and therefore minimize side effects.[2,3] Computational models also have served as hypothesis generators and testing grounds for new methods of neurostimulation, such as coordinated reset neuromodulation,[4] phase-specific stimulation,[5] and linear delayed feedback stimulation.[6] In some cases, computational predictions have proven exceedingly accurate in animal and human studies.[7–9]

Despite the value of computational modeling, many basic biophysical contributions thereto are not well known to the clinical neuromodulation community. The goal of this article is to introduce computational modeling of DBS, synthesizing information from studies that have used computational modeling to elucidate the biophysical principles, parameters, and mechanisms of neurostimulation.

### Biophysics of DBS—An Overview

DBS begins at the implantable pulse generator (IPG), the energy storing component of DBS devices. When a stimulation pulse is generated, electrons flow through the circuitry between the IPG and electrode(s). At the electrode-tissue interface, there is a transition from electron flow to ion flow that is mediated by either reversible nonfaradaic capacitive coupling or irreversible faradaic

Address correspondence to: Patrick R. Ng, BS, BA, Harvard Medical School, 25 Shattuck St, Boston, MA 02115, USA. Email: patrickrayng@gmail.com

[1] Harvard Medical School, Boston, MA, USA;
[2] Department of Neurosurgery, Massachusetts General Hospital, Boston, MA, USA;
[3] Department of Biomedical Engineering, Duke University, Durham, NC, USA; and
[4] Department of Neurosurgery, Duke University, Durham, NC, USA

For more information on author guidelines, an explanation of our peer review process, and conflict of interest informed consent policies, please see the journal's Guide for Authors.

Source(s) of financial support: The authors reported no funding sources.

oxidation-reduction reaction (Table 1).[10] Current, or the rate of flow of electrically charged particles such as electrons or ions through a medium, passes through the tissue and creates a distribution of electric potentials. An electric field is thereby generated between a positive anode and a negative cathode. The electric field is applied to a three-dimensional region populated with neural processes (cell bodies, axons, and dendrites) and triggers the opening of voltage-gated ion channels. If the stimulus is strong enough, an action potential is propagated, causing the release of either excitatory or inhibitory neurotransmitters.

Extracellular stimulation nondiscriminately affects three classes of neurons that surround the implanted electrode: local cells, afferent inputs, and fibers of passage.[11] Local cells are neurons that have their somata near the electrode and project axons locally and/or to a different brain region (Fig. 1). In the context of subthalamic nucleus (STN) DBS, local cells are STN projection neurons. Afferent inputs, such as the hyperdirect motor tract to the STN, are neurons that project to the region around the electrode and have synaptic connections with local cells. Fibers of passage, such as the dentatorubrothalamic tract that passes posterior medial to the STN, are neurons that project axonal processes through the region around the electrode and have cell bodies and axon terminals far from the electrode contact.

## Overview of Computational Models of DBS

Computational models are computer-based mathematical simulations of complex systems. Although computational models enable highly controlled investigations of assorted variables within the system, these models are built on, and inevitably limited by, sets of assumptions. Computational models typically emerge once a critical mass of experimental and clinical data has been collected, data that are used to parameterize, constrain, and validate the models.

Accordingly, computational models of DBS emerged in parallel with the clinical development of DBS (Fig. 2). Louis Lapicque introduced one of the first mathematical models of the neuron in 1907 with his "integrate-and-fire" model, describing membrane voltage as a function of input current.[25] In 1952, Hodgkin and Huxley used voltage clamp electrodes to measure the electrical activity of squid giant axons and developed the first biophysical model of the action potential, representing neurons as biological circuits with capacitance, conductance, and membrane potentials.[16] In the late 1950s, Wilfrid Rall created the first multicompartmental model of the neuron using cable theory and went on to derive the first theoretical exploration of dendrites and spines.[17] In the 1970s, McNeal was the first to develop techniques for modeling neural responses to extracellular stimulation.[18] These

**Table 1.** Basic Terms Related to the Biophysics of DBS.

| Term | Definition |
|---|---|
| Nonfaradaic capacitive coupling (double layer charging) | Electrons build up on or are deplated from the electrode and positively/negatively charged ions accumulate near the metal surface. |
| Faradaic oxidation-reduction reaction | Electrons are transferred or captured directly from the electrode to a reactant in the tissue. |
| VTA | An estimated three-dimensional space around the electrode, where the produced extracellular electric field can initiate an action potential on a neural process. |
| Conductivity | A material's ability to conduct an electric field; the reciprocal of electrical resistivity. |
| Tissue Conductivity | A tissue's ability to conduct an electric field; determined by homogeneity vs inhomogeneity and isotropy vs anisotropy. |
| Homogeneity vs inhomogeneity | The spatial consistency of the electrical properties of a given tissue. Inhomogeneous or heterogeneous tissues have conductivities that depend on distance from the extracellular current source. Boundaries, such as gray and white matter transition zones have high inhomogeneity. |
| Isotropy vs anisotropy | The uniformity of electrical properties in all orientations of the tissue. Anisotropic tissues have conductivities that depend on fiber direction or orientation. |
| Tissue capacitance | The tissue's ability to store electric charge. Determined by the dielectric constant and permittivity of the tissue medium. |
| Size-specific activation | Preferential activation based on axon diameter. |
| Orientation-specific activation | Preferential activation based on orientation of neural elements (axons of passage, terminating axons, local neurons) relative to the electrode shaft. |
| Impedance | The total opposing force to the current flow in an alternating circuit. |
| Electrode impedance | The total opposing force to current flow that arises from the encapsulation layer around the electrode. Determined by the thickness and conductivity of the encapsulation layer around the electrode and by the conductivity of the bulk tissue medium. |
| Current steering | CCS with multiple independent current sources. |
| Synaptic suppression ("information lesion" effect) | The disruption of the synaptic communication between the directly stimulated presynaptic neuron and the postsynaptic neuron. |
| Reinforcement loop mechanism | Extracellular stimulation elicits different neural network perturbations that when delivered at the right frequency reinforce each other. This reinforcement within the targeted neural loops may restore normal activity within the network. |
| Neuronal class selectivity | Preferential activation of specific neuronal classes (local cells, afferent inputs, fibers of passage). |
| Neural process selectivity | Preferential activation of specific neural processes (dendrites, cell bodies, axons). |
| Chronaxie | The pulse width needed to stimulate a nerve fiber using an electric current twice rheobase, the minimal current amplitude of infinite duration required to elicit a threshold response; often visualized on a strength-duration or amplitude-pulse width curve. |



  

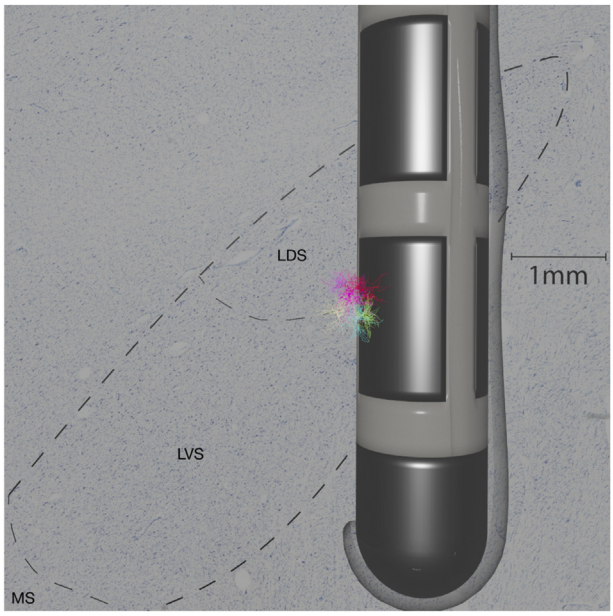


**Figure 1.** Close-up of Boston Vercise directional DBS lead (DB-2202-45) implanted in the STN. The composition was created with Blender (version 2.79b, Blender Foundation, Amsterdam, The Netherlands). Electrode encapsulation is represented as a semitransparent surface on the right and bottom sides of the electrode. A Nissl-stained coronal slice of a woman aged 34 years and neurotypical, obtained from the Allen Brain Atlas,[12] is shown to scale as background. The STN and its subdomains (lateroventral subthalamic nucleus [LDS], lateroventral subthalamic nucleus [LVS], and medial subthalamic nucleus [MS]) are outlined with dashed lines. A three-dimensional model of a rat thalamic relay cell[13] was scaled to match the typical dimensions of human STN dendritic arbors, which can extend up to 600 mm from the soma.[14] A cluster of five neurons is shown in relation to the DBS contacts. For visual clarity, the distance between somas of the depicted neurons is roughly double that of neighboring neurons in the human STN, resulting in one-eighth the real neural density. [Color figure can be viewed at www.neuromodulationjournal.org]

milestones are just a few of the landmark discoveries that have laid the groundwork for the study of neurostimulation with computational neurosciences.

In general, computational models of DBS are constructed from two basic components: a model of the electric field generated by the implanted electrode and a model of the stimulated neuron. Models of the electric field range in complexity. Early electric field models assumed a point-source electrode in an infinite homogenous isotropic medium (Table 1).[26] Subsequent studies have indicated the limitations of excluding variables such as anisotropy, heterogeneity, and the electrode-tissue interface (Table 1).[27] More recent electric field models are more complex, using finite-element method volume conductors with explicit representations of time dependence, electrode geometry, tissue inhomogeneity, and tissue anisotropy. Multicompartment cable models, which represent neurons as electrical circuits with conductance, capacitance, and intracellular resistance, are commonly used to model the stimulated neuron.[11] Although representing neurons as electrical circuits is the most common modeling approach, neurons also can be mathematically represented as oscillators (ie, coupled oscillator models) or represented at a population level (ie, mean-field models) (presented in the later section, Network Models of DBS and Closed-Loop Modeling). Combining a model of the electric field and a model of the stimulated neuron enables predictions of the neuronal response to extracellular stimulation.[18] In some cases, anatomical models, derived from variables extracted from imaging and histologic studies, can be incorporated into DBS models, allowing patient-specific predictions of neural responses.[2,28]

There are several methods for combining models of the electric field and stimulated neurons. Field-cable models use our current biophysical understanding of the underlying mechanisms to simulate physiology and include explicit representations of the electric field, axonal trajectories, and transmembrane ion channels.[18] The cost of these detailed models is a larger computational demand that requires significant computational infrastructure. Alternative approaches limit the amount of biophysical complexity incorporated into the model by deriving some metric from the electric field that predicts activation on the basis of assumptions regarding the behavior of neurons. The upside of decreased complexity is decreased computational burden and increased practicality. All computational models of DBS manage this tradeoff in different ways. For example, the driving-force method implements one degree of simplification relative to field-cable models, comprising detailed calculations of the electric field and simplified estimates of the transmembrane response.[29,30] The driving-force method is well suited for DBS models that include tractography, or representations of axonal pathways.[31] Rattay showed that the predicted response of an individual neuron to an electric field is related to the activating function—the second derivative of the extracellular potential distribution along each neural process.[32] This work is a key example of how complex biophysical phenomena can be simulated with relatively simple methods. Although the activating-function–based approaches allow general calculations of neural activation, there also are prediction errors associated with this technique.[29,33,34]

The volume of tissue activated (VTA) method further simplifies representations of the electric field and neuronal response and is the most frequently used approach in clinical applications. The VTA is a three-dimensional estimate of stimulus spread and is constructed by identifying axons that are suprathreshold for activation (Table 1).[35] There are several methods for determining VTA, but two major techniques include either calculating the activating function or defining an electric field threshold, which is the first derivative of the extracellular potential distribution.[28,35–37] VTA predictions can be improved with different computational techniques, such as artificial neural networks.[38] VTAs have been shown to be sufficiently accurate in assisting clinical decision making,[19,39] but these predictions are limited by the variables incorporated into the model.[40] VTA models are the least biophysically realistic of the techniques mentioned and are known to overestimate the stimulus spread, with potential errors in the extent of activation to the order of millimeters.[28] Despite these inaccuracies, VTA-based approaches are the most used models in clinical applications (presented in the section on Clinical Applications), owing in large part to the decreased computational burden and increased usability that come with simplified models. Practitioners therefore should note that the VTA is not a "ground truth" but simply an estimate of neural activation based on the specific modeling techniques and decisions made by the respective investigators.

As with any methods, computational models of DBS have limitations. For instance, models may assume that a stimulated region contains neurons with uniform membrane dynamics, myelination, and morphology when this homogeneity may not exist in vivo.[41] This assumption would affect predictions of which neurons produce action potentials. Furthermore, given the complexity of neural circuitry in vivo, models may omit certain fiber tracts to focus on a particular pathway, although these ignored interactions may be



  

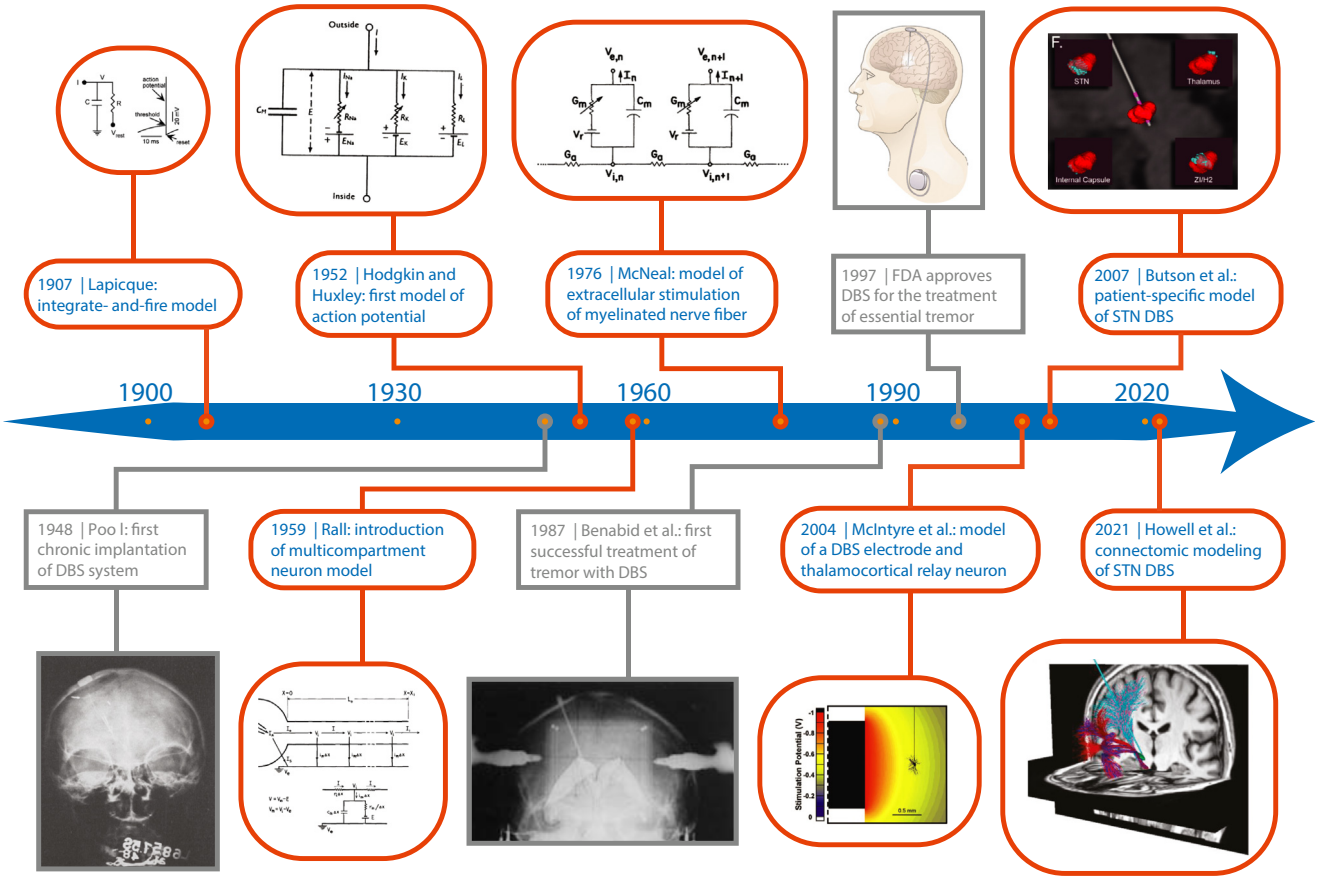


**Figure 2.** Timeline of milestones related to the clinical development (gray) and computational modeling (orange) of DBS. One of the earliest computational models of the neuron was created by Louis Lapicque, who represented the neuron as an electric circuit with a parallel capacitor and resistor.[15] Nearly 50 years later, Alan Hodgkin and Andrew Huxley used experimental data from squid giant axons to derive the first computational model of the action potential.[16] Models of the neuron grew in complexity with contributions from computational neuroscientists, such as Wilfrid Rall, who created the multicompartment neuron model.[17] The techniques for modeling neural responses to extracellular stimulation were established by Donald McNeal.[18] Since then, computational models have become increasingly personalized to individual patients.[19,20] Recently, connectomic modeling has been achieved.[21] Progress in neuro-computational modeling paralleled clinical breakthroughs in the development of DBS.[22–24] FDA, Food and Drug Administration. [Color figure can be viewed at www.neuromodulationjournal.org]

important.[42] Moreover, other cell types that regulate neuronal activation, such as glial cells, typically are excluded from models.[43] These examples show that computational models can be limited not only by the omission of certain inputs but also by fundamental knowledge gaps about the system being modeled. Despite these limitations, computational models of DBS have catalyzed important insights about the relationships between different biophysical parameters and extracellular stimulation, as will be discussed in later sections.

## Biophysics of DBS—The Electrode

DBS electrodes have undergone many permutations. In a study by Benabid et al, which heralded the modern era of DBS, neurostimulation was delivered via a single contact electrode.[22] For two subsequent decades, the standard electrode was a cylindrical quadripolar probe with a 1.27 mm diameter and four contacts, each measuring 1.5 mm in length and spaced 0.5 or 1.5 mm apart.[44] Today, the most commonly used electrodes have similar dimensions but are "directional," with the two center contacts segmented into three separate contacts each, for a total of eight contacts. Computational models have shown that innovations focused on electrode and contact design affect biocompatibility, energy efficiency, the VTA, and ultimately the neural response (Table 2).

### Material Properties

When a DBS pulse is delivered, electrical charge is injected into the surrounding tissue through either reversible nonfaradaic capacitive coupling or irreversible faradaic oxidation-reduction reaction.[10] Charge is the product of amplitude (ie, the maximum magnitude of stimulation per pulse) and pulse duration. The charge injection capacity is defined as the maximum charge density that can be applied to the surface of the electrode without the formation of reactive radical species that can cause tissue damage.[49] Material-based tissue damage is grounded on both the likelihood of generating reactive radical species at the electrode-tissue interface and the biocompatibility of the material (ie, the tendency to incite a foreign body response).[50] Therefore, different materials, including those used in the coating of electrodes, have certain advantages and limitations in their ability to support charge injection and moderate adverse tissue responses.[51,52] Modern leads contain contacts made from platinum–iridium, which minimizes toxicity and optimizes conductivity (Table 1), and nickel alloy connectors encased in a polyurethane sheath.[44]

Electrode capacitance (Table 1) is a function of electrode material and size.[53] According to computational models, electrode capacitance influences the shape of the stimulus waveform, resulting in a decay of the current applied to the tissue, during



  

**Table 2.** Summary of Biophysical Parameters, Dependencies, and Effects in DBS.

| Category | Biophysical parameter | Common options | Dependent on: | Affects: |
|---|---|---|---|---|
| Electrode | Material | Platinum/platinum–iridium, iridium oxide, tantalum/tantalum oxide, PEDOT, carbon nanotubes | • Electrode and contact design | • Biocompatibility<br>• Electrode capacitance<br>• Waveform of VCS<br>• VTA of VCS |
| | Contact size and shape | Standard electrode (cylindrical contacts)<br>Segmented electrode (rectangular or elliptical contacts) | • Aspect ratio (height/diameter)<br>• Surface area<br>• Perimeter | • Current density at electrode surface<br>• Tissue damage<br>• Orientation-specific activation<br>• Size-specific activation<br>• VTA<br>• Energy efficiency |
| | Contact segmentation | Commercially available systems:<br>• St. Jude Medical Infinity System<br>• Boston Scientific Vercise System<br>• Medtronic SenSight System | • Contact size, shape, and placement | • Size-specific activation<br>• Orientation-specific activation<br>• VTA |
| Stimulation parameters | Frequency | High frequency (>100 Hz), typically 130 Hz<br>Low frequency (<100 Hz) | • Intrinsic frequency of target neurons | • Therapeutic efficacy<br>• Neuronal class selectivity<br>• Information lesion effect<br>• Reinforcement loop mechanism<br>• VTA |
| | Current vs voltage control | VCS<br>CCS | VCS<br>• Dependent on electrode capacitance and electrode impedance<br>CCS<br>• Dependent on tissue capacitance | |
| | Amplitude | General strategy of increasing amplitude in steps of 0.1–0.5 V or 0.1–0.5 mA up to a max of 5 V, 5 mA, or when side effects occur[45] | VCS<br>• Dependent on amount of voltage delivered by IPG<br>CCS<br>• Dependent on amount of current delivered by IPG | • Neural process selectivity<br>• VTA |
| | Pulse width | Start with 60 μs<br>Consider using shorter pulse width <60 μs to counteract side effects | Conventional DBS systems<br>• 60μs–450μs<br>Vercise DBS system<br>• 20μs–450μs | • VTA<br>• Size-specific activation<br>• Distance-specific activation<br>• Energy efficiency<br>• DBS dosage |
| | Monopolar vs bipolar | Monopolar stimulation<br>Bipolar stimulation | • Electrode and contact design | • Orientation-specific activation<br>• VTA<br>• Electrode impedance |
| | Anodic vs cathodic | Anodic stimulation<br>Cathodic stimulation | • Electrical configuration of the IPG and electrode | • Neuronal class selectivity<br>• Orientation-specific activation |
| | Waveform | Rectangular waveforms<br>Symmetrical charge-balanced<br>Asymmetrical charge-balanced | • Amplitude<br>• Pulse width<br>• Cathodic or anodic stimulation | • Electrode corrosion<br>• Tissue damage<br>• Neuronal class selectivity<br>• Chronaxie<br>• Energy efficiency |
| Substrate | Electrode encapsulation | 5–500-μm–thick fibrous encapsulation layer[46] | • Neuroinflammatory response to implantation<br>• Biocompatibility | • Electrode impedance<br>• VCS<br>• VTA of VCS |

*(Continued)*

**Table 2.** *Continued*

| Category | Biophysical parameter | Common options | Dependent on: | Affects: |
|---|---|---|---|---|
| | | | • Mechanical stress | • Waveform<br>• Energy efficiency |
| | Tissue conductivity | Mean conductivity for gray matter[47]: 0.47 S/m<br>Mean conductivity for white matter[47]: 0.22 S/m | • Homogeneity vs inhomogeneity<br>• Isotropy vs anisotropy | • VTA |
| | Axon fiber size | Axon diameters are approximately 4–5 μm[48] | • Contact size<br>• Pulse width<br>• Distance from electrode | • VTA<br>• Therapeutic effect |
| | Axon fiber orientation | Variable | • Contact size<br>• Contact shape<br>• Contact segmentation<br>• Monopolar vs bipolar<br>• Anodic vs cathodic | • Therapeutic effect |

PEDOT, poly(3,4-ethylene dioxythiophene).

voltage-controlled stimulation and therefore modulates the spatial spread of the electric field.[39,53] In vitro and animal studies have validated the effects of electrode capacitance on the stimulus waveform and VTA.[54] The impact of electrode capacitance on voltage-controlled stimulation is one reason for modern DBS devices transitioning to using current-controlled stimulation, which is discussed in later sections.[55] Although not currently available in clinical DBS electrodes, alternative coatings and materials, such as carbon nanotubes and poly(3,4-ethylenedioxythiophene) hybrid materials, can be used to increase the charge-carrying capacity of the electrode.[52]

### Electrode and Contact Design

Electrode design alters the current density at the electrode surface, the VTA, the selectivity of which neurons (based on size and orientation) are activated, and the power efficiency of the lead. McIntyre and Grill observed that surface area, radius of curvature of the electrode tip, and the presence of a resistive coating all influenced the magnitude of the current density along the surface of the electrode.[51] A more uniform current density minimizes stimulation-induced neural damage, which has been proposed to result from the formation of reactive radical species.[49,51] Regarding the physical dimensions of the electrode contacts, computational studies have shown that a low contact aspect ratio (diameter to height) can maximize the VTA.[35] Contact size also can be used to control orientation-specific activation (Table 1)[56,57] and size-specific activation (Table 1),[56] enabling preferential targeting of certain fibers. One computational study found that a contact size of approximately 5.76 $mm^2$ may optimize energy efficiency while circumventing limitations in charge density.[56] Other studies have shown that contact shape, as determined by surface area and perimeter layout, affects energy efficiency[58,59] and orientation-specific activation.[59] Therefore, depending on the application and target structure, electrode and contact design can be leveraged to minimize tissue injury, increase power efficiency, and generate a more precise VTA and neural response.

### Segmented Electrodes and Directional DBS

Historical quadripolar DBS electrodes had cylindrical contacts that generated rotationally symmetrical electrical fields assuming circumferentially symmetric tissue impedance. In addition, most DBS devices were designed to deliver single-source voltage-controlled cathodic stimulation (Table 1). If adequate therapeutic effects were not achieved, multicontact strategies could be trialed. However, there are two limitations with this approach. First, electrode impedance (Table 1), which has been shown to fluctuate over time after implantation (presented in the section on Electrode Encapsulation), can affect the consistency of current delivered by voltage-controlled stimulation.[60] Second, although quadripolar cylindrical electrodes enable the electric field to be shaped along the axis of the lead with different combinations of anodic and cathodic currents, the targeting of specific structures in the horizontal plane is limited. Therefore, directional electrodes with segmented contacts (Fig. 1) were created that can more precisely sculpt the electric field in the plane perpendicular to the lead.

Computational studies have defined the potential benefits of directional DBS. These simulation experiments have shown that 1) current steering (Table 1) is unaffected by electrode impedance; 2) balancing current flow through adjacent cathodes can increase the VTA size relative to monopolar stimulation; and 3) current steering could improve the preferential targeting of specific neural



  

populations in STN DBS for Parkinson's disease (PD).[61,62] Computational models have indicated that segmented electrodes can sculpt the VTA with submillimeter precision to target only specific nuclei or fiber pathways, thereby maximizing therapeutic benefits and minimizing adverse effects.[63] Other studies have shown that directional segmented electrodes can achieve both size-specific and orientation-specific activation.[3,64] Animal studies have confirmed that directional DBS can improve VTA precision and that orientation-specific activation can enable improved treatment responses.[63,65] Indeed, clinical trials have verified that directional DBS can increase side-effect thresholds while achieving symptomatic benefits comparable with those of conventional DBS, paving a new path for hardware development.[66]

## Biophysics of DBS—Stimulation Parameters

Stimulation parameters are often selected empirically on the basis of clinical experience, expert consensus, or trained habits. There has been growing discussion about moving away from the conventional mode of stimulation—continuous, cathodic, monopolar, high-frequency stimulation—and exploring pathology- and brain-region specific protocols, which would form the foundation for technologies such as closed-loop stimulation. Computational modeling has helped catalyze this shift toward precision DBS by offering a first-principles approach to identifying the effects of stimulation parameters (Table 2, Fig. 3) on the electric field. These insights can help clinicians select optimized stimulation paradigms a priori, as opposed to the current workflow of trial and error.

### Frequency

Stimulation frequency is defined as the number of stimulation pulses per second (Fig. 3a). Since Benabid et al[22] showed the utility of high-frequency (>100 Hz) DBS, which mimics the effects of lesional surgery, for tremor in PD, continuous high-frequency stimulation has been used for several conditions, including PD, dystonia, essential tremor, epilepsy, pain, obsessive-compulsive disorder, depression, Tourette syndrome, and Alzheimer's disease, with varying degrees of efficacy.[67] Low-frequency stimulation also has been trialed for some conditions, such as epilepsy and pain.[67] Stimulation frequency is a critical parameter given symptom relief and adverse effects have been shown to be strongly associated with frequency.[68,69]

Computational models have helped elucidate how frequency modulates the effects of neurostimulation. DBS efficacy has been shown to depend on stimulation frequency, with the optimal frequency correlated with the intrinsic frequency of target neurons.[70] Furthermore, high-frequency pulses may decouple the firing activity of the soma and of the axon and may generate efferent outputs at the stimulus frequency in most neurons within 2 mm of the electrode contact.[20] Furthermore, models of STN DBS have shown that high-frequency stimulation may disconnect hyperdirect neurons—cortical layer V pyramidal neurons that send collaterals from their corticofugal axons to the STN—from the cortical circuitry.[71] This synaptic suppression or information lesion effect (Table 1), which only occurs at high frequencies, may prevent the generation or propagation of the pathological synchronized oscillations found in PD and has been proposed as a general mechanism for DBS.[71] Indeed, network models have shown that DBS suppresses pathological oscillations and internal globus pallidus (Gpi) bursting only at certain stimulus frequencies.[72,73] In summary, 1) the efficacy of DBS depends on both stimulation frequency and the intrinsic frequency of target neurons; 2) stimulation frequency can determine neuronal class

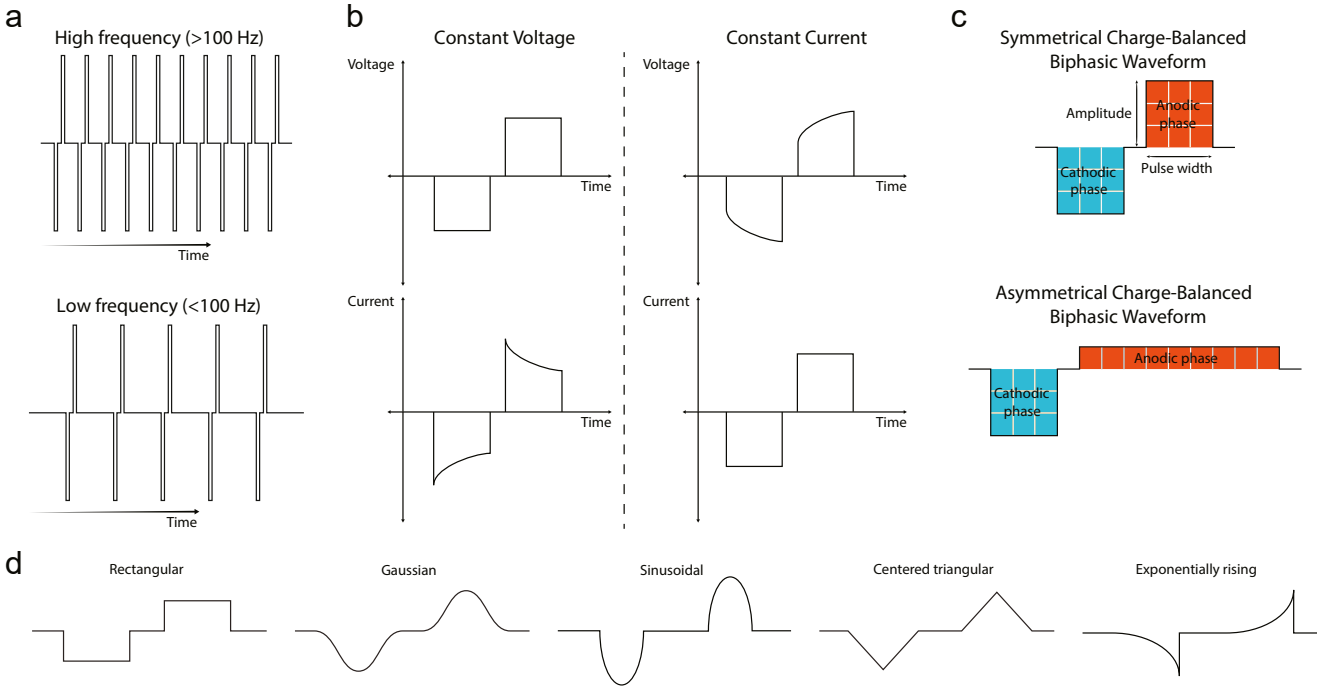


**Figure 3.** Schematics of stimulation parameters. a. Stimulation frequency is typically set >100 Hz, but low-frequency stimulation also has been applied in some cases. b. With VCS (constant voltage), current will not be constant, whereas with CCS (constant current), voltage will not be constant. c. With charge-balanced waveforms, the net total amount of charge injected into the tissue (shaded area under the curve) will be zero. Whether a charge-balanced waveform is symmetrical or asymmetrical depends on whether the cathodic and anodic phases have identical (symmetrical) or nonidentical (asymmetrical) amplitudes and pulse widths. d. Waveforms of different morphology are presented. [Color figure can be viewed at www.neuromodulationjournal.org]



  

selectivity (Table 1); and 3) some hypothesized mechanisms of DBS are frequency-dependent.

### Voltage-Controlled Stimulation vs Current-Controlled Stimulation

IPGs may be programmed to deliver either voltage-controlled (VCS) or current-controlled stimulation (CCS) (Fig. 3b), although historically, DBS systems were restricted to VCS. Voltage is defined as the difference in electric potential between two points, whereas current is defined as the rate of flow of electrically charged particles such as electrons or ions through a medium. In VCS, voltage is held constant, and the amount of current that flows through the tissue is determined by the impedance, or resistance, of the entire circuit. The overall impedance is based on the aggregate resistance of the extension wire, lead wire, electrode-tissue interface, electrode encapsulation, and surrounding tissue.[50] In CCS, a constant amount of current is delivered to the tissue and is not influenced by the circuit impedance.[50]

Computational models have shown that VCS is dependent on electrode capacitance and electrode impedance (Table 1) (presented in Material Properties and Electrode Encapsulation sections). Specifically, models that integrate finite-element–based solutions of the electric field and multicompartment cable models of myelinated axons have shown that during VCS, electrode capacitance and electrode impedance affect the shape of the waveform and spread of the VTA.[53,60] More complex patient-specific models that incorporate data from both anatomical and diffusion tensor magnetic resonance imaging (MRI) to refine simulations of the electric field and stimulated neurons have confirmed the effects of electrode capacitance and electrode impedance on the waveform and VTA during VCS.[39] The dependence of VCS on electrode capacitance and impedance also has been observed in in vitro and in animal studies.[54,74] In a work by Lempka et al,[74] which studied VCS in nonhuman primates, postimplantation changes in the electrode-tissue interface increased electrode impedance, whereas stimulation itself caused an initial decrease in electrode impedance. Impedance-related fluctuations in the electric field generated by VCS might explain programming adjustments during the first several weeks after DBS implantation.[75] Indeed, clinical studies in patients with long-term implanted DBS systems have reported fluctuations in electrode impedance that largely stabilize by six months.[76]

Computational studies also have explored CCS. Although CCS is relatively unaffected by electrode capacitance, combined finite-element models of the electric field and multicompartment cable models of axons have shown that tissue capacitance (Table 1) influences the VTA generated by CCS.[53] However, compared with electrode capacitance and impedance, tissue capacitance is unlikely to change substantially over time and among patients, which may explain why VTAs generated by CCS are more consistent and easier to sculpt to an anatomic target (presented in Segmented Electrodes and Directional DBS).[53,61,62] These findings also have been supported by in vitro and animal experiments.[54,74] Lempka et al[74] revealed three advantages of CCS over VCS: 1) a more consistent stimulation effect without voltage fluctuations during initial programming; 2) more consistent comparisons of parameter settings within and across patients; and 3) a reduction in confounding variables when studying the effects of DBS onset. Indeed, the INTREPID trial provided class I evidence for using a multiple independent contact current-controlled device in STN DBS.[77] Although there are still no randomized head-to-head trials of CCS vs VCS, most modern devices primarily use CCS.[55]

### Amplitude

Amplitude is defined as the maximum magnitude of stimulation per pulse, measured in either voltage or current depending on whether VCS or CCS is used (Fig. 3c). Relative to other energy-equivalent parameter changes, amplitude has the greatest effect on PD motor symptoms and is the most adjusted parameter during the initial programming of STN DBS.[68] Titrating voltage or current determines the amplitude, depending on whether the IPG delivers VCS or CCS.

Computational models have shown that amplitude influences neural process selectivity (Table 1) and affects the VTA. Early models of extracellular point-source stimulation of idealized single neurons illustrated that changing amplitude could alter the site of action potential initiation when the electrode is positioned near the cell body.[78] Subsequent models incorporating electrode and tissue capacitance, in addition to anatomically relevant anisotropy/inhomogeneity, have all shown that amplitude affects the spread of the VTA.[38,53] Clinically, a study of direct brain stimulation in patients with epilepsy confirmed that amplitude alters the magnitude of stimulatory responses and the spread of activation across broad cortical regions.[79] During initial programming, amplitude is titrated up to determine the threshold of beneficial effects, then further increased to detect the threshold of adverse effects.[75]

### Pulse Width

Pulse width is defined as the duration of the stimulation pulse (Fig. 3c). Conventional DBS systems allow pulse widths ranging from 60 μs to 450 μs. Newer devices, such as the Vercise DBS system (Boston Scientific, Marlborough, MA), have enabled shorter pulse widths (<60 μs).

Computational models have helped delineate the effects of pulse width on DBS. First, models have illustrated how pulse width, like amplitude, modulates the amount of charge delivered to the tissue and subsequently the spread of the VTA.[38,80] Short pulse widths can selectively activate distant large-diameter fibers, whereas long pulse widths can selectively activate nearby small-diameter fibers.[64] Furthermore, computational and animal studies have shown that pulse width influences energy efficiency.[64,81] Anderson et al observed that the energetically optimal pulse width is the chronaxie of an axon (Table 1).[64]

Pulse widths have been historically initiated at 60 μs, the lower-bound setting of conventional systems, for STN DBS.[68] Recent studies have shown that shorter pulse widths (<60 μs) can increase therapeutic windows in both STN and ventral intermediate nucleus (VIM) stimulation by decreasing side effects.[82,83] Although these investigators proposed that improvements arose from shorter pulse widths preferentially activating small nearby (therapeutic) fibers and avoiding larger distant (adverse) fibers, a computational study by Anderson et al suggested that smaller VTAs drove the observed benefits.[64] This assertion needs to be confirmed, but the computational result indicates the potential of modeling to evaluate mechanisms of clinically observed outcomes.

### Monopolar vs Bipolar Stimulation

Monopolar stimulation involves the flow of current from one contact in the target region to another contact in the IPG. In bipolar stimulation, current flows between two contacts in the target region. Early computational studies showed no difference in neural process selectivity between monopolar and bipolar electrodes.[84] In contrast, recent studies have shown that the choice of monopolar



  

vs bipolar stimulation can influence orientation-specific activation.[85] Assuming an isotropic, homogenous medium, monopolar stimulation produces a spherical, relatively large VTA around the electrode, whereas bipolar stimulation creates a more focused, localized VTA.[26,38] The choice of monopolar or bipolar stimulation also can modulate the shape of the electric field,[3,38] in addition to orientation-specific activation of fibers.[3] Lastly, models generated by Butson et al predict that bipolar stimulation leads to higher electrode impedance relative to monopolar stimulation, which is relevant to the charge density when using impedance-dependent VCS and to energy consumption when using CCS.[60] In clinical practice, the initial default is monopolar configuration, which typically requires less charge injection than does bipolar stimulation to achieve comparable clinical results. However, if monopolar stimulation cannot generate an appropriately large therapeutic window, bipolar stimulation is typically initiated, which has utility in minimizing adverse effects.[75]

### Anodic vs Cathodic Stimulation

In cathodic stimulation, electrons flow from the negative cathode (an electrode contact) to the positive anode (IPG or an electrode contact). In anodic stimulation, electrons flow from the positive anode (IPG or an electrode contact) to the negative cathode (an electrode contact). Early animal studies showed that anodic stimulation required approximately three to eight times more current to elicit an action potential from myelinated fibers.[86] On the basis of these findings, most modern DBS applications use monopolar cathodic stimulation, with the IPG serving as the anode.

Computational studies have offered a more nuanced picture. Early models showed that monophasic cathodic stimuli selectively activate fibers of passage over cell bodies, whereas monophasic anodic stimuli selectively activate cell bodies over fibers of passage.[84] A more recent study by Anderson et al[85] showed that the choice of cathodic vs anodic stimulation can facilitate orientation-specific activation. These findings explain the results of a recent randomized clinical trial of STN stimulation in patients with PD, which showed that although anodic stimulation required greater therapeutic and side-effect thresholds (ie, higher charge injection) than did cathodic stimulation, anodic stimulation offered a wider therapeutic window and better motor symptom reduction within this window.[87] Models created by Anderson et al[85] suggest that these clinical improvements may result from preferential anodic stimulation of appropriately oriented fibers. Another clinical study showed tremor improvements from biphasic stimulation of the VIM, possibly owing to the anodic phase activating nearby orthogonal axons.[88] Depending on the clinical application, cathodic, anodic, or a mixed configuration may be considered.

### Waveform

Waveforms describe the stimulation current or voltage as a function of time (Fig. 3c,d**)**. Waveforms can be classified as monophasic, biphasic, or polyphasic. A monophasic waveform contains a single unidirectional pulse from baseline to either a positive or negative value, whereas biphasic waveforms have two pulses with opposite sign. Polyphasic waveforms are bidirectional waves with at least three different pulses. Symmetrical biphasic waveforms have pulses of equal duration and amplitude, whereas asymmetrical biphasic waveforms have pulses of unequal duration and amplitude. Charge-balanced waveforms prevent net charge injection into the tissue. Charge is the product of amplitude and pulse duration.

With chronic stimulation waveforms, charge balancing is essential to minimize electrode degradation and tissue damage.[89,90] As mentioned previously, during a stimulation pulse, current is passed from the electrode to the tissue through either reversible nonfaradaic capacitive coupling or irreversible faradaic oxidation-reduction reaction. Importantly, the irreversible chemical reactions are the source of the reactive radical species that cause stimulation-induced adverse effects. Therefore, methods to minimize these irreversible reactions are crucial to ensuring sustained safety of chronic stimulation. With monophasic pulses, the electrode potential tends to drift away from the open-circuit electrode potential, creating an increased probability of accumulating irreversible faradaic reactions compared with charge-balanced, biphasic pulses. Although irreversible reactions can still occur with charge-balanced waveforms, the likelihood is substantially lower because the second charge-balancing pulse brings the electrode potential closer to the open-circuit electrode potential.[90]

Computational studies have substantiated the effects of waveform on DBS. Models suggest that relative to monophasic stimuli, charge-balanced biphasic waveforms can decrease the probability of electrode corrosion and tissue damage.[84] The protective properties of biphasic stimuli have been confirmed in animal studies.[91] In contrast, symmetrical charge-balanced pulses cannot produce the neuronal class selectivity achieved by asymmetrical charge-balanced waveforms.[84] Animal studies suggest that asymmetrical stimulation can indeed modulate the spatiotemporal dynamics of the neural response, depending on whether the primary phase is cathodic or anodic.[92] Still, in a pilot study comparing symmetrical biphasic pulses with conventional DBS pulses (high-amplitude short stimulation pulses [cathodal phase] followed by low-amplitude long recharge periods [anodal phase]) in eleven patients with essential tremor, symmetrical biphasic pulses resulted in significantly better tremor control.[88] Furthermore, modifying the interpulse gap or pulse phase order of a waveform also can dramatically alter the efficiency of neuronal activation and entrainment.[93] In addition, waveform selection can affect the chronaxie.[53] Lastly, stimulation waveform influences the efficiency of the IPG, which has important implications for battery life, frequency of battery replacements, and size of DBS devices. Computational models have suggested that nonrectangular waveforms, such as exponential Gaussian, sinusoidal, and centered-triangular waveforms, can be more energy-efficient than the rectangular pulses of conventional systems (Fig. 3d).[94] In summary, waveform affects the potential for tissue injury, neuronal class selectivity, efficiency of neuronal activation, the chronaxie, and energy efficiency.

## Biophysics of DBS—The Substrate

Neural responses to DBS are governed by the biophysical characteristics of the substrate itself. The properties of the brain tissue that affect DBS include the encapsulation layer around the electrode, tissue conductivity, and the neuronal characteristics of the target and adjacent structures (Table 2, Fig. 1).

### Electrode Encapsulation

Surgical implantation of DBS electrodes causes acute and chronic biomechanical changes to the local tissue environment.[95,96] During and shortly after implantation, there is tissue and vascular damage,



  

which induces a neuroinflammatory response including the recruitment of microglia and astrocytes to the site of injury and edema formation. Over several weeks, a foreign body reaction ensues. A fibrous encapsulation layer of inflammatory cells and deposited extracellular components and proteins forms on and around the electrode. The neuronal density around the electrode initially decreases, creating a neuronal gap that may be refilled over time. Over the long term, a stable glial scar forms around the electrode. Nevertheless, micromotions, device biocompatibility, tethering of the implant, and mechanical stress can contribute to a chronic inflammatory response, which can potentially cause persistent blood-brain–barrier leakage that interferes with electrode function.[95,97]

Computational models have established the effects of these reactive tissue changes on the VTA, stimulation waveform, and efficiency of DBS. As discussed in the previous section on Voltage-Controlled Stimulation, the encapsulation layer (Fig. 1) surrounding the electrode modifies electrode impedance. Models have shown that the thickness, conductivity, and capacitance of the encapsulation layer alter the VTA of VCS.[39,60] Postimplantation changes to the electrode-brain interface (EBI) also modulate the waveform shape and amplitude differently at short- and long-term stages of implantation.[39,98] Lastly, EBI impedance can influence stimulation efficiency.[59] These findings have been recapitulated in in vitro and animal studies.[54,59] Innovations in biomaterials and coatings that elicit a weaker foreign body response may minimize fluctuations in electrode impedance.[52]

### Tissue Conductivity

The electrical properties of brain tissue significantly influence the effects of DBS.[99] Although difficult to measure, tissue conductivity is a key electrical property and is frequently characterized by two qualities: homogeneity vs inhomogeneity and isotropy vs anisotropy (Table 1). The former refers to the consistency in space of electrical properties in a tissue, and the latter refers to the uniformity of electrical properties in all orientations of the tissue. An inhomogeneous or heterogeneous tissue has a conductivity that is dependent on location or distance from the extracellular current source (ie, the electrode), whereas an anisotropic tissue has a conductivity that is dependent on direction or orientation.[26] Not surprisingly, gray matter, white matter, and cerebrospinal fluid show heterogeneous tissue conductivities as determined through direct resistivity recordings.[100] Therefore, areas of gray matter/white matter transition have high degrees of inhomogeneity. The anisotropy of tissue conductivities is more difficult to measure. Classically, cerebrospinal fluid and gray matter were assumed to be isotropic and all white matter anisotropic. These conclusions are possibly true at macroscopic length scales but do not hold at microscopic length scales. For example, gray matter contains cell bodies, neuropil, myelinated axons, and blood vessels and should therefore have some degree of anisotropy.[101] Furthermore, the assumption of white matter anisotropy was based on early measurements of fibers with homogeneous trajectories (ie, the internal capsule and dorsal column of the spinal cord), whereas in reality, white matter can contain fiber tracts with many different orientations.[86,102,103] Shimony et al[104] and Tuch et al[105] developed more accurate methods of determining anisotropy and estimating tissue conductivity with diffusion tensor MRI via cross-property relations. These approximations have suggested, for example, that the thalamus has a relatively low anisotropy and inhomogeneity whereas the subthalamic nucleus has a relatively high anisotropy and inhomogeneity.[54,104]

Computational models have helped identify the effects of tissue conductivity on the voltage distribution of DBS. Early computational work by Grill showed that tissue inhomogeneity and anisotropy can shape the generated electric field, the stimulation current thresholds for neural excitation, and the subsequent neural response.[106] Subsequent computational studies of STN DBS confirmed that anisotropy and inhomogeneity of surrounding tissues such as the internal capsule and zona incerta can distort the size and shape of the VTA.[26] Indeed, stimulation thresholds and the number of axons activated by an extracellular stimulation can vary on the basis of the local anisotropy and heterogeneity.[80] Some studies have suggested that anisotropy more significantly affects the VTA and stimulation thresholds than does heterogeneity.[103] These findings have been validated in animal studies.[54] Computational models that incorporate inhomogeneity and anisotropy could predict side effects observed in patients.[39] Patient-specific models that incorporate individual tissue conductivity values from magnetic resonance electrical impedance tomography are on the horizon.[107]

### Axon Fiber Size and Orientation

Axon fibers are known targets of extracellular stimulation.[84] Axon size and alignment affect not only whether an action potential is conducted but also which targets are appropriate for selective stimulation. For example, therapeutic benefit in STN DBS has been associated with small-diameter nearby fibers, whereas side effects have been associated with large-diameter distant fibers.[64] The influence of fiber size and orientation on neural responses to extracellular stimulation is difficult to assess in vivo but can be comprehensively evaluated with computational models. Early work by McNeal[18] established that the stimulation threshold of an axon is directly proportional to the distance from the electrode and inversely proportional to the fiber diameter. Subsequent computational studies confirmed that the neural response to DBS depends on the position and orientation of the axon relative to the electrode,[20,80] in addition to fiber diameter.[80] Increasing axon diameter also can increase the VTA.[38] Regarding size- and orientation-specific activation, as discussed in previous sections, contact design, directional DBS, pulse width, monopolar vs bipolar stimulation, and anodic vs cathodic stimulation can all be designed to preferentially target fibers of specific size and orientation, thereby optimizing the benefits of DBS.

## Future Directions

### Network Models of DBS and Closed-Loop Modeling

Most of this review has thus far focused on the biophysical parameters of DBS at the level of local neural elements and nerve fibers. Although computational models have made significant progress in identifying the relationships between these local parameters and neurostimulation, modeling techniques also have elucidated the wider network effects of DBS, which are critical to understand, especially as investigators begin to develop models of closed-loop stimulation. One approach to creating a network model of DBS is called a neural network model, which involves three main components: 1) biophysical neuronal models, which are represented as circuit components with capacitance, conductance, and membrane potentials, grouped together into the different nodes of the network architecture (eg, the thalamus, STN, external globus pallidus [Gpe], and Gpi for the basal ganglia network); 2)



  

excitatory or inhibitory connections between the nodes; and 3) DBS pulses modeled as input sources of current injection and activation at the target node (eg, the STN for STN DBS). Complexity of the network model depends on the number and type of neuronal models included, the dynamics of the connections between nodes, and the stimulatory relationship between DBS pulses and the target node activity.[108] It should be noted that there are numerous other computational techniques to model neural networks, such as mean-field models[109] and coupled oscillator models.[4,110] Some caveats of neural network models include heavy computational burden as more neurons or nodes are added to the model and difficulties with acquiring robust physiological data with which to parameterize the models.[108]

Although network models have been used to study the effects of DBS on several neurological disorders, including PD,[111] epilepsy,[112,113] and depression,[114] models of PD have been the most widely studied and will therefore serve as an example. Albin et al helped establish the initial descriptive model of the basal ganglia, detailing the excitatory and inhibitory connections between different nodes of the circuit.[115] With a simplified neural network model, Montgomery and Baker hypothesized that stimulation creates a noise source of neural activity that disrupts pathological bursting within the basal ganglia, improving information transfer between the basal ganglia and cortex.[116] Rubin and Terman created the first biophysical network model of the basal ganglia, inspiring an entire generation of in silico architectures for this brain circuit. The Rubin and Terman model includes mathematical representations of the neuronal populations in the thalamus, STN, Gpe, and Gpi. Studies with this model showed that STN DBS may normalize abnormal oscillations within the basal ganglia and restore normal thalamic and cortical processing of sensorimotor inputs.[42] Subsequent network models parameterized with experimental data from parkinsonian nonhuman primates confirmed that signaling between different brain regions, specifically the cortical-basal-ganglia-thalamocortical loop, may contribute to both the pathophysiology and DBS-elicited restoration of disordered parkinsonian brain circuits.[72,117,118]

These computational network models can be further adapted to include the feedback signal of a closed-loop DBS system as an input of the model. Traditionally, DBS is delivered in an open-loop fashion with continuous electrical impulses. Closed-loop DBS involves delivering stimulation as a function of sensed real-time neuronal activity. A closed-loop or adaptive DBS system includes three modules: a sensing module that evaluates the feedback signal, a control module that analyzes the signal and defines the new stimulation parameters, and a stimulation module that delivers the stimulation.[119] Compared with open-loop DBS, closed-loop stimulation can potentially decrease the adverse effects of continuous stimulation, while also optimizing therapeutic benefits and decreasing battery consumption.[119] For PD, beta activity of the STN is a well-supported feedback control biomarker, though other network and external biomarkers are under investigation.[119] Computational network models have facilitated several advances in the development of closed-loop DBS. For example, the performance of different control modules can be evaluated in detail with network models.[120–123] Furthermore, computational analyses can help define and test novel closed-loop stimulation strategies, such as linear/nonlinear delayed feedback stimulation and multisite linear delayed feedback stimulation, all of which involve the modulation of pulse amplitudes based on different feedback signals.[124–126] Network models also have shown promise in refining existing stimulatory techniques, such as proposing a new method of combining phase-locked and adaptive DBS strategies.[5] Taken together, computational network models are proven tools that will likely play critical roles in shaping the future of closed-loop neurostimulation.

### Connectomic Modeling

Another recent advance in computational techniques that has been used to investigate the network effects of DBS is connectomic modeling. Modern neuroscience has progressed from "localizing" neurological functions to discrete brain regions to conceptualizing function as a product of network-based activity.[127] Innovations in imaging techniques, such as functional MRI (fMRI) and diffusion tensor imaging (DTI), have catalyzed insights on the functional and structural connectivity, respectively, of the brain.[127] In silico connectomic DBS modeling involves combining 1) a model of the neural structures affected by stimulation (ie, different pathway-activation models such as the VTA, driving-force models, and field-cable models)[28] and 2) functional and/or structural connectivity maps. The pathway-activation model serves as the seed region to correlate stimulation with affected brain regions.[128] The complexity of the pathway-activation model determines the accuracy of the larger connectomic model.[28] With approaches that use functional connectivity maps, a key assumption is that stimulating a brain region also will affect the regions that are functionally connected.[127]

In silico connectomic models are beginning to affect the clinical practice of DBS. With sufficient electrical and anatomical detail incorporated into the computational architecture, connectomic models can effectively predict recruitment dynamics of white matter pathways.[21] Combining connectomic models with clinical outcome data can help identify potential therapeutic targets.[127] These models have retrospectively pinpointed sweetspot and white matter tract targets, in addition to optimal connectivity patterns, for DBS in patients with PD,[129,130] essential tremor,[131] depression,[132] Tourette syndrome,[133] epilepsy,[134] chronic cluster headaches,[135] dystonia,[136] and Alzheimer's disease.[137] Connectomic model-based target selection also has been applied prospectively to cohorts of patients with depression[138] and obsessive-compulsive disorder[139] and resulted in relatively high responder rates, though sample sizes were not powered to make definitive claims of efficacy.

Connectomic models bear some technical limitations. Most connectomic models have used VTA calculations, the limitations of which are discussed in previous sections. Furthermore, current connectivity imaging modalities—primarily fMRI and DTI—are susceptible to distortion artifacts, registration errors, and insufficient spatial resolution.[127] Some studies have used functional connectivity maps from large cohorts of healthy participants to address limitations in sample size.[136,137] There is current debate about differences in the connectivity profiles of these normative populations vs disease-matched patients and about the value of normative maps in connectomic modeling and surgical planning.[140,141] In addition, unlike the computational network models previously described (presented in the section on Network Models of DBS and Closed-Loop Modeling), connectomic models do not currently incorporate the excitatory and/or inhibitory synaptic influences between different brain regions. Gunalan et al[28] recommended incorporating these dynamical network analyses into connectomic techniques in the future.



  

**Table 3.** Commercial and Academic VTA Visualization Tools Available to the Clinical Neuromodulation Community.

| Commercial or academic | Tool | Source | Methods | Clinical application | Intraoperative or postoperative visualization | Limitations |
|---|---|---|---|---|---|---|
| Commercial | SureTune™ | Medtronic Inc | Astrom et al[36] (2015) | • Probabilistic outcome brain mapping based on SureTune™ robustly predicted clinical improvements in patients with cervical dystonia and with pallidal DBS[148] | Postoperative | • Homogenous, isotropic tissue assumptions[36]<br>• Inaccurate VTAs with current control stimulation[149]<br>• Inaccurate VTAs in tissue with cerebrospinal fluid[149] |
| | GUIDE™ XT (older version) or STIMVIEW™ XT (newer version) | Boston Scientific | Miocinovic et al[142] (2007) (Cicerone) | • GUIDE™ XT-guided programming reduced programming time without compromising outcomes compared with traditional protocols for patients with PD[146,147,150] | Postoperative | • Homogenous, isotropic tissue assumptions[149] |
| Academic | LiU DBS modeling software application | Johansson et al[151] (2019) | Astrom et al[36] (2015) | • ELMA application from the LiU software was used to identify targets for OCD DBS[152] | Postoperative | • Axons assumed to be oriented in straight lines that are tangential to the electrode surface[149]<br>• Pulse frequency and perielectrode conductivity changes not included in the model[149] |
| | OSS-DBS | Butenko et al[153] (2020) | Butenko et al[153] (2020) | • No clinical studies using VTAs generated by OSS-DBS published to date | Postoperative | • Limited data sets on some parameters, such as thickness of the encapsulation layer[153]<br>• Long computation time, though can be mitigated by parallel computations[153] |
| | Lead-DBS | Horn et al[154] (2019) | Four types of VTA models[130,155–157]<br>• Kuncel et al[155] (2008)<br>• Mädler and Coenen[156] (2012)<br>• Dembek et al[66,157] (2017)<br>• Horn et al[130] (2017) | • Lead-DBS models identified potential targets for PD,[158] dystonia,[136] multiple sclerosis tremor,[159] Alzheimer's disease[137] | Postoperative | • Not as biophysically complex as other models[103] |
| | Lead-OR | Oxenford et al[160] (2022) | Dembek et al[66,157] (2017) | • No clinical studies using VTAs generated by Lead-OR published to date | Intraoperative | • Isotropic tissue assumptions[157]<br>• Spherical VTA[157] |
| | PaCER | Husch and Petersen[161] (2018) | Mädler and Coenen[156] (2012) | • No clinical studies using VTAs generated by PaCER published to date | Postoperative | • Isotropic tissue assumptions[156]<br>• Spherical VTA[156] |
| | DBSproc | Lauro et al[162] (2016) | Mädler and Coenen[156] (2012) | • DBSproc models identified the tractography patterns associated with therapeutic benefit in patients with PD DBS[163] | Postoperative | • Isotropic tissue assumptions[156]<br>• Spherical VTA[156] |
| | StimVision | Noecker et al[132] (2018) | Chaturvedi et al[38] (2013) | • StimVision models enabled intraoperative tractography-based | Intraoperative and postoperative | • Isotropic tissue[38] |

*(Continued)*

**Table 3.** *Continued*

| Commercial or academic | Tool | Source | Methods | Clinical application | Intraoperative or postoperative visualization | Limitations |
|---|---|---|---|---|---|---|
| | | | | targeting for subcallosal cingulate DBS for depression[132] | | • Assumption of straight axons perpendicular to electrode[38] |
| | ImageVis3D Mobile | Butson et al[144] (2013) | Butson et al[144] (2013) | • ImageVis3D enabled safe and efficacious home health management of PD DBS in a randomized clinical trial[164] | Postoperative | • Fixed pulse width and frequency settings[144]<br>• Pre-computed visualizations and selection of lead location in advance[165] |
| | Duality | Vorwerk et al[165] (2020) | Butson and McIntyre[35] (2006) | • No clinical studies using VTAs generated by Duality published to date | Intraoperative and postoperative | • Homogenous, isotropic tissue assumptions[35]<br>• Does not incorporate encapsulation layer[35] |
| | FastField | Baniasadi et al[166] (2020) | Astrom et al[36] (2015) | • FastField models identified potential targets for writer's cramp,[167] essential tremor,[168] and treatment-resistant bulimic anorexia nervosa[169] | Postoperative | • Homogenous tissue[166]<br>• Does not support bipolar stimulation[166] |

LiU, Linköping University; OSS, open-source simulation.

Clinical Applications

Computational models are not only tools that can elucidate the mechanisms of DBS but also powerful adjuncts that can improve clinical practice. In Frankemolle et al, the Cicerone software system[142] generated patient-specific computational DBS models with visualizable VTAs for patients with advanced PD. Stimulation parameters were chosen on the basis of either clinical assessments (ie, the conventional trial-and-error workflow) or model-based overlap between the VTA and both target and off-target regions. Compared with clinically determined parameters, model-based parameters enabled equivalent improvements in Unified Parkinson's Disease Rating Scale (UPDRS) III scores, significantly better cognitive-motor performance, and decreased power consumption.[143] Similarly positive results were found with *ImageVis3D Mobile*, a computational model-based visualization system that can be operated on point-of-care mobile devices such as iPhones or iPads. Stimulation settings chosen by this system, which generates VTAs relative to surrounding structures, were similar to those chosen by the standard of care, yet the model-based workflow consumed significantly less time.[144] In fact, the Graphical User Interface for DBS Evaluation (GUIDE) study, a multicenter prospective study with blinded UPDRS-III examinations, compared DBS programming with either a computational model derived from the Dimension ® software (Intelect Medical Inc, Boston, MA) or traditional workflows. The study found that UPDRS-III score improvements were not significantly different between the model-based and traditional workflows; however, less time and less power were required with the model-based approach.[145] A randomized, double-blind, controlled crossover study by Lange et al confirmed that model-based protocols derived from the GUIDE™ XT module in the *Brainlab Elements* software suite (Brainlab, Munich, Germany) significantly reduced programming time without compromising symptom control and patient satisfaction compared with traditional protocols after four weeks of stimulation for patients with PD.[146] Waldthaler et al[147] confirmed that GUIDE™ XT-guided approaches are just as effective as standard-of-care approaches with directional DBS programming for patients with PD. These studies suggest that computational models and their resultant visualization tools can significantly improve the efficiency of DBS programming, primarily by focusing the stimulatory programming parameter space, which contains a vast range of permutations.

Most clinical applications of computational models have centered on using VTA visualizations to guide programming or identify therapeutic targets. Table 3 presents a list of some commercial and academic VTA visualization tools that are currently available to the neuromodulation community. Although clinical utility has been achieved with many of these algorithms, these VTA-based tools are often built on simplified computational models that lack the highest level of biophysical complexity (eg, incorporation of tissue conductivity, encapsulation layers, and titratable stimulation parameters). The upside of sacrificing biophysical complexity in these VTA visualization tools is decreased computational time and more efficient clinical usability.

As the next generation of model-based tools emerges, technical advances will facilitate bringing more complex models to the bedside. For example, parallel processing and client-server systems have been shown to reduce computational times.[153,165] More sophisticated patient-facing tools that do not solely rely on VTA visualizations are already present. For example, the second version of StimVision (Table 3), StimVision v2, replaces the VTA method for predicting the neural response to stimulation with the driving-force

method, incorporating more detailed representations of the electric field and axonal trajectories. Although the driving-force method still lacks the complexity of field-cable models, which are the gold standard for biophysical realism, StimVision v2 can create models within two minutes, and future versions could reduce this computational time to a few seconds.[170] As indicated in Table 3, though most clinical applications of computational models are currently implemented in the postoperative stage when the lead location is confirmed and registered within the respective model, there are now algorithms, such as Lead-OR,[160] StimVision,[132] and Duality,[165] that can create near real-time representations of the lead and estimated stimulation spread, enabling more interactive intraoperative planning.

Improved sensor capabilities, such as accelerometers that can quantitatively measure tremor severity, may further augment the utility of model-based visualization tools. For instance, Shah et al used patient-specific models of the electric field and accelerometer-based measurements of tremor to create three-dimensional digital visualizations of the anatomic regions with the greatest tremor improvements and worst adverse effects, known respectively as the patient's improvement maps and adverse effect maps. These "stimulation maps" showed promise in simplifying the process of optimizing lead placement and initial parameter selection for patients with essential tremor.[171] Lastly, automation has begun to affect not only the creation of computational models[153] but also model-based selection of programming settings based on optimal activation of target tissue.[172] Taken together, computational models are poised to significantly influence the clinical practice of neuromodulation.

## CONCLUSIONS

DBS involves a complex interaction between the implanted electrode, stimulation parameters, and the neural substrate, all of which are governed by several biophysical factors. Although there are many variables that contribute to extracellular neurostimulation, computational models are powerful in silico tools for understanding DBS at both the local and network levels. Given that software based on computational models currently inform clinical practice, understanding the biophysical principles on which they are based is increasingly relevant for the clinical neuromodulation community. Future directions of computational DBS modeling include network models of closed-loop stimulation, connectomic modeling, and clinically applicable simulations with increasing accuracy and predictive value.

### Authorship Statements

Patrick R. Ng and Robert Mark Richardson conceptualized the project. Patrick R. Ng wrote the manuscript with input from Alan Bush, Matteo Vissani, Cameron C. McIntyre, and Robert Mark Richardson. Patrick R. Ng, Alan Bush, and Matteo Vissani created the figures and tables. All authors approved the final manuscript.

### Conflict of Interest

Cameron C. McIntyre is a paid consultant for Boston Scientific Neuromodulation, receives royalties from Hologram Consultants, Neuros Medical, and Qr8 Health, and is a shareholder in the following companies: Hologram Consultants, Surgical Information Sciences, BrainDynamics, CereGate, Autonomic Technologies, Cardionomic, and Enspire DBS. The remaining authors reported no conflict of interest.


### How to Cite This Article

Ng P.R., Bush A., Vissani M., McIntyre C.C., Richardson R.M. 2024. Biophysical Principles and Computational Modeling of Deep Brain Stimulation.
Neuromodulation 2024; 27: 422–439.


## REFERENCES


1. Ellis TM, Foote KD, Fernandez HH, et al. Reoperation for suboptimal outcomes after deep brain stimulation surgery. *Neurosurgery*. 2008;63:754–760. https://doi.org/10.1227/01.NEU.0000325492.58799.35 [discussion: 760].
2. Butson CR, Cooper SE, Henderson JM, Wolgamuth B, McIntyre CC. Probabilistic analysis of activation volumes generated during deep brain stimulation. *NeuroImage*. 2011;54:2096–2104. https://doi.org/10.1016/j.neuroimage.2010.10.059.
3. Slopsema JP, Peña E, Patriat R, et al. Clinical deep brain stimulation strategies for orientation-selective pathway activation. *J Neural Eng*. 2018;15, 056029. https://doi.org/10.1088/1741-2552/aad978.
4. Tass PA. A model of desynchronizing deep brain stimulation with a demand-controlled coordinated reset of neural subpopulations. *Biol Cybern*. 2003;89:81–88. https://doi.org/10.1007/s00422-003-0425-7.
5. Weerasinghe G, Duchet B, Cagnan H, Brown P, Bick C, Bogacz R. Predicting the effects of deep brain stimulation using a reduced coupled oscillator model. *PLoS Comput Biol*. 2019;15, e1006575. https://doi.org/10.1371/journal.pcbi.1006575.
6. Popovych OV, Tass PA. Adaptive delivery of continuous and delayed feedback deep brain stimulation - a computational study. *Sci Rep*. 2019;9, 10585. https://doi.org/10.1038/s41598-019-47036-4.
7. Adamchic I, Hauptmann C, Barnikol UB, et al. Coordinated reset neuromodulation for Parkinson's disease: proof-of-concept study. *Mov Disord*. 2014;29:1679–1684. https://doi.org/10.1002/mds.25923.
8. Cagnan H, Pedrosa D, Little S, et al. Stimulating at the right time: phase-specific deep brain stimulation. *Brain*. 2017;140:132–145. https://doi.org/10.1093/brain/aww286.
9. Brocker DT, Swan BD, So RQ, Turner DA, Gross RE, Grill WM. Optimized temporal pattern of brain stimulation designed by computational evolution. *Sci Transl Med*. 2017;9, eaah3532. https://doi.org/10.1126/scitranslmed.aah3532.
10. Kumsa DW, Bhadra N, Hudak EM, Kelley SC, Untereker DF, Mortimer JT. Electron transfer processes occurring on platinum neural stimulating electrodes: a tutorial on the i(V e) profile. *J Neural Eng*. 2016;13, 052001. https://doi.org/10.1088/1741-2560/13/5/052001.
11. Mcintyre CC, Foutz TJ. Computational modeling of deep brain stimulation. *Handb Clin Neurol*. 2013;116:55–61. https://doi.org/10.1016/B978-0-444-53497-2.00005-X.
12. Ding SL, Royall JJ, Sunkin SM, et al. Comprehensive cellular-resolution atlas of the adult human brain. *J Comp Neurol*. 2016;524:3127–3481. https://doi.org/10.1002/cne.24080.
13. Barthó P, Slézia A, Varga V, et al. Cortical control of zona incerta. *J Neurosci*. 2007;27:1670–1681. https://doi.org/10.1523/JNEUROSCI.3768-06.2007.
14. Bergman H. *The Hidden Life of the Basal Ganglia: At the Base of Brain and Mind*. The MIT Press; 2021.
15. Abbott LF. Lapicque's introduction of the integrate-and-fire model neuron (1907). *Brain Res Bull*. 1999;50:303–304. https://doi.org/10.1016/s0361-9230(99)00161-6.
16. Hodgkin AL, Huxley AF. A quantitative description of membrane current and its application to conduction and excitation in nerve. *J Physiol*. 1952;117:500–544. https://doi.org/10.1113/jphysiol.1952.sp004764.
17. Rall W. Branching dendritic trees and motoneuron membrane resistivity. *Exp Neurol*. 1959;1:491–527. https://doi.org/10.1016/0014-4886(59)90046-9.
18. McNeal DR. Analysis of a model for excitation of myelinated nerve. *IEEE Trans Biomed Eng*. 1976;23:329–337. https://doi.org/10.1109/TBME.1976.324593.
19. Butson CR, Cooper SE, Henderson JM, McIntyre CC. Patient-specific analysis of the volume of tissue activated during deep brain stimulation. *NeuroImage*. 2007;34:661–670. https://doi.org/10.1016/j.neuroimage.2006.09.034.
20. McIntyre CC, Grill WM, Sherman DL, Thakor NV. Cellular effects of deep brain stimulation: model-based analysis of activation and inhibition. *J Neurophysiol*. 2004;91:1457–1469. https://doi.org/10.1152/jn.00989.2003.
21. Howell B, Isbaine F, Willie JT, et al. Image-based biophysical modeling predicts cortical potentials evoked with subthalamic deep brain stimulation. *Brain Stimul*. 2021;14:549–563. https://doi.org/10.1016/j.brs.2021.03.009.
22. Benabid AL, Pollak P, Louveau A, Henry S, de Rougemont J. Combined (thalamotomy and stimulation) stereotactic surgery of the VIM thalamic nucleus for




  

bilateral Parkinson disease. *Appl Neurophysiol*. 1987;50:344–346. https://doi.org/10.1159/000100803.
23. Pool JL. Psychosurgery in older people. *J Am Geriatr Soc*. 1954;2:456–466. https://doi.org/10.1111/j.1532-5415.1954.tb02138.x.
24. Premarket Approval (PMA). U.S. Food and Drug Administration. https://www.accessdata.fda.gov/scripts/cdrh/cfdocs/cfPMA/pma.cfm?id=P960009. Accessed September 23, 2022.
25. Lapicque L. Recherches quantitatives sur l'excitation électrique des nerfs traitée comme une polarization. *Journal de physiologie et de pathologie générale*. 1907;9:620–635.
26. McIntyre CC, Mori S, Sherman DL, Thakor NV, Vitek JL. Electric field and stimulating influence generated by deep brain stimulation of the subthalamic nucleus. *Clin Neurophysiol*. 2004;115:589–595. https://doi.org/10.1016/j.clinph.2003.10.033.
27. McIntyre CC, Miocinovic S, Butson CR. Computational analysis of deep brain stimulation. *Expert Rev Med Devices*. 2007;4:615–622. https://doi.org/10.1586/17434440.4.5.615.
28. Gunalan K, Howell B, McIntyre CC. Quantifying axonal responses in patient-specific models of subthalamic deep brain stimulation. *NeuroImage*. 2018;172:263–277. https://doi.org/10.1016/j.neuroimage.2018.01.015.
29. Warman EN, Grill WM, Durand D. Modeling the effects of electric fields on nerve fibers: determination of excitation thresholds. *IEEE Trans Biomed Eng*. 1992;39:1244–1254. https://doi.org/10.1109/10.184700.
30. Peterson EJ, Izad O, Tyler DJ. Predicting myelinated axon activation using spatial characteristics of the extracellular field. *J Neural Eng*. 2011;8:046030. https://doi.org/10.1088/1741-2560/8/4/046030.
31. Howell B, Gunalan K, McIntyre CC. A driving-force predictor for estimating pathway activation in patient-specific models of deep brain stimulation. *Neuromodulation*. 2019;22:403–415. https://doi.org/10.1111/ner.12929.
32. Rattay F. Analysis of models for external stimulation of axons. *IEEE Trans Biomed Eng*. 1986;33:974–977. https://doi.org/10.1109/TBME.1986.325670.
33. Zierhofer CM. Analysis of a linear model for electrical stimulation of axons–critical remarks on the "activating function concept". *IEEE Trans Biomed Eng*. 2001;48:173–184. https://doi.org/10.1109/10.909638.
34. Moffitt MA, McIntyre CC, Grill WM. Prediction of myelinated nerve fiber stimulation thresholds: limitations of linear models. *IEEE Trans Biomed Eng*. 2004;51:229–236. https://doi.org/10.1109/TBME.2003.820382.
35. Butson CR, McIntyre CC. Role of electrode design on the volume of tissue activated during deep brain stimulation. *J Neural Eng*. 2006;3:1–8. https://doi.org/10.1088/1741-2560/3/1/001.
36. Astrom M, Diczfalusy E, Martens H, Wardell K. Relationship between neural activation and electric field distribution during deep brain stimulation. *IEEE Trans Biomed Eng*. 2015;62:664–672. https://doi.org/10.1109/TBME.2014.2363494.
37. Duffley G, Anderson DN, Vorwerk J, Dorval AD, Butson CR. Evaluation of methodologies for computing the deep brain stimulation volume of tissue activated. *J Neural Eng*. 2019;16:066024. https://doi.org/10.1088/1741-2552/ab3c95.
38. Chaturvedi A, Luján JL, McIntyre CC. Artificial neural network based characterization of the volume of tissue activated during deep brain stimulation. *J Neural Eng*. 2013;10:056023. https://doi.org/10.1088/1741-2560/10/5/056023.
39. Chaturvedi A, Butson CR, Lempka SF, Cooper SE, McIntyre CC. Patient-specific models of deep brain stimulation: influence of field model complexity on neural activation predictions. *Brain Stimul*. 2010;3:65–67. https://doi.org/10.1016/j.brs.2010.01.003.
40. Butson CR, McIntyre CC. The use of stimulation field models for deep brain stimulation programming. *Brain Stimul*. 2015;8:976–978. https://doi.org/10.1016/j.brs.2015.06.005.
41. Sweet JA, Pace J, Girgis F, Miller JP. Computational modeling and neuroimaging techniques for targeting during deep brain stimulation. *Front Neuroanat*. 2016;10:71. https://doi.org/10.3389/fnana.2016.00071.
42. Rubin JE, Terman D. High frequency stimulation of the subthalamic nucleus eliminates pathological thalamic rhythmicity in a computational model. *J Comput Neurosci*. 2004;16:211–235. https://doi.org/10.1023/B:JCNS.0000025686.47117.67.
43. Miocinovic S, Parent M, Butson CR, et al. Computational analysis of subthalamic nucleus and lenticular fasciculus activation during therapeutic deep brain stimulation. *J Neurophysiol*. 2006;96:1569–1580. https://doi.org/10.1152/jn.00305.2006.
44. Krauss JK, Lipsman N, Aziz T, et al. Technology of deep brain stimulation: current status and future directions. *Nat Rev Neurol*. 2021;17:75–87. https://doi.org/10.1038/s41582-020-00426-z.
45. Koeglsperger T, Palleis C, Hell F, Mehrkens JH, Bötzel K. Deep brain stimulation programming for movement disorders: current concepts and evidence-based strategies. *Front Neurol*. 2019;10:410. https://doi.org/10.3389/fneur.2019.00410.
46. DiLorenzo DJ, Jankovic J, Simpson RK, Takei H, Powell SZ. Neurohistopathological findings at the electrode-tissue interface in long-term deep brain stimulation: systematic literature review, case report, and assessment of stimulation threshold safety. *Neuromodulation*. 2014;17:405–418. https://doi.org/10.1111/ner.12192 [discussion: 418].
47. McCann H, Pisano G, Beltrachini L. Variation in reported human head tissue electrical conductivity values. *Brain Topogr*. 2019;32:825–858. https://doi.org/10.1007/s10548-019-00710-2.
48. Huang SY, Tian Q, Fan Q, et al. High-gradient diffusion MRI reveals distinct estimates of axon diameter index within different white matter tracts in the in vivo human brain. *Brain Struct Funct*. 2020;225:1277–1291. https://doi.org/10.1007/s00429-019-01961-2.
49. Rose TL, Robblee LS. Electrical stimulation with Pt electrodes. VIII. Electrochemically safe charge injection limits with 0.2 ms pulses. *IEEE Trans Biomed Eng*. 1990;37:1118–1120. https://doi.org/10.1109/10.61038.
50. Brocker DT, Grill WM. Principles of electrical stimulation of neural tissue. *Handb Clin Neurol*. 2013;116:3–18. https://doi.org/10.1016/B978-0-444-53497-2.00001-2.
51. McIntyre CC, Grill WM. Finite element analysis of the current-density and electric field generated by metal microelectrodes. *Ann Biomed Eng*. 2001;29:227–235. https://doi.org/10.1114/1.1352640.
52. Fattahi P, Yang G, Kim G, Abidian MR. A review of organic and inorganic biomaterials for neural interfaces. *Adv Mater*. 2014;26:1846–1885. https://doi.org/10.1002/adma.201304496.
53. Butson CR, McIntyre CC. Tissue and electrode capacitance reduce neural activation volumes during deep brain stimulation. *Clin Neurophysiol*. 2005;116:2490–2500. https://doi.org/10.1016/j.clinph.2005.06.023.
54. Miocinovic S, Lempka SF, Russo GS, et al. Experimental and theoretical characterization of the voltage distribution generated by deep brain stimulation. *Exp Neurol*. 2009;216:166–176. https://doi.org/10.1016/j.expneurol.2008.11.024.
55. Bronstein JM, Tagliati M, McIntyre C, et al. The rationale driving the evolution of deep brain stimulation to constant-current devices. *Neuromodulation*. 2015;18:85–88. https://doi.org/10.1111/ner.12227 [discussion: 88–89].
56. Anderson DN, Dorval AD, Rolston JD, Pulst SM, Anderson CJ. Computational investigation of the impact of deep brain stimulation contact size and shape on neural selectivity. *J Neural Eng*. 2021;18. https://doi.org/10.1088/1741-2552/abeeaa.
57. Howell B, Huynh B, Grill WM. Design and *in vivo* evaluation of more efficient and selective deep brain stimulation electrodes. *J Neural Eng*. 2015;12, 046030. https://doi.org/10.1088/1741-2560/12/4/046030.
58. Grill WM, Wei XF. High efficiency electrodes for deep brain stimulation. *Annu Int Conf IEEE Eng Med Biol Soc*. 2009;2009:3298–3301. https://doi.org/10.1109/IEMBS.2009.5333774.
59. Howell B, Grill WM. Evaluation of high-perimeter electrode designs for deep brain stimulation. *J Neural Eng*. 2014;11:046026. https://doi.org/10.1088/1741-2560/11/4/046026.
60. Butson CR, Maks CB, McIntyre CC. Sources and effects of electrode impedance during deep brain stimulation. *Clin Neurophysiol*. 2006;117:447–454. https://doi.org/10.1016/j.clinph.2005.10.007.
61. Butson CR, McIntyre CC. Current steering to control the volume of tissue activated during deep brain stimulation. *Brain Stimul*. 2008;1:7–15. https://doi.org/10.1016/j.brs.2007.08.004.
62. Chaturvedi A, Foutz TJ, McIntyre CC. Current steering to activate targeted neural pathways during deep brain stimulation of the subthalamic region. *Brain Stimul*. 2012;5:369–377. https://doi.org/10.1016/j.brs.2011.05.002.
63. Martens HCF, Toader E, Decré MMJ, et al. Spatial steering of deep brain stimulation volumes using a novel lead design. *Clin Neurophysiol*. 2011;122:558–566. https://doi.org/10.1016/j.clinph.2010.07.026.
64. Anderson CJ, Anderson DN, Pulst SM, Butson CR, Dorval AD. Neural selectivity, efficiency, and dose equivalence in deep brain stimulation through pulse width tuning and segmented electrodes. *Brain Stimul*. 2020;13:1040–1050. https://doi.org/10.1016/j.brs.2020.03.017.
65. Slopsema JP, Canna A, Uchenik M, et al. Orientation-selective and directional deep brain stimulation in swine assessed by functional MRI at 3T. *NeuroImage*. 2021;224:117357. https://doi.org/10.1016/j.neuroimage.2020.117357.
66. Dembek TA, Reker P, Visser-Vandewalle V, et al. Directional DBS increases side-effect thresholds-a prospective, double-blind trial. *Mov Disord*. 2017;32:1380–1388. https://doi.org/10.1002/mds.27093.
67. Cagnan H, Denison T, McIntyre C, Brown P. Emerging technologies for improved deep brain stimulation. *Nat Biotechnol*. 2019;37:1024–1033. https://doi.org/10.1038/s41587-019-0244-6.
68. Dayal V, Limousin P, Foltynie T. Subthalamic nucleus deep brain stimulation in Parkinson's disease: the effect of varying stimulation parameters. *J Parkinsons Dis*. 2017;7:235–245. https://doi.org/10.3233/JPD-171077.
69. Moro E, Esselink RJA, Xie J, Hommel M, Benabid AL, Pollak P. The impact on Parkinson's disease of electrical parameter settings in STN stimulation. *Neurology*. 2002;59:706–713. https://doi.org/10.1212/wnl.59.5.706.
70. Grill WM, Snyder AN, Miocinovic S. Deep brain stimulation creates an informational lesion of the stimulated nucleus. *Neuroreport*. 2004;15:1137–1140. https://doi.org/10.1097/00001756-200405190-00011.
71. Anderson RW, Farokhniaee A, Gunalan K, Howell B, McIntyre CC. Action potential initiation, propagation, and cortical invasion in the hyperdirect pathway during subthalamic deep brain stimulation. *Brain Stimul*. 2018;11:1140–1150. https://doi.org/10.1016/j.brs.2018.05.008.
72. Hahn PJ, McIntyre CC. Modeling shifts in the rate and pattern of subthalamopallidal network activity during deep brain stimulation. *J Comput Neurosci*. 2010;28:425–441. https://doi.org/10.1007/s10827-010-0225-8.
73. Holt AB, Netoff TI. Origins and suppression of oscillations in a computational model of Parkinson's disease. *J Comput Neurosci*. 2014;37:505–521. https://doi.org/10.1007/s10827-014-0523-7.
74. Lempka SF, Johnson MD, Miocinovic S, Vitek JL, McIntyre CC. Current-controlled deep brain stimulation reduces in vivo voltage fluctuations observed during



  

voltage-controlled stimulation. *Clin Neurophysiol*. 2010;121:2128–2133. https://doi.org/10.1016/j.clinph.2010.04.026.
75. Volkmann J, Moro E, Pahwa R. Basic algorithms for the programming of deep brain stimulation in Parkinson's disease. *Mov Disord*. 2006;21(suppl 14):S284–S289. https://doi.org/10.1002/mds.20961.
76. Wong J, Gunduz A, Shute J, et al. Longitudinal follow-up of impedance drift in deep brain stimulation cases. *Tremor Other Hyperkinet Mov (N Y)*. 2018;8:542. https://doi.org/10.7916/D8M62XTC.
77. Vitek JL, Jain R, Chen L, et al. Subthalamic nucleus deep brain stimulation with a multiple independent constant current-controlled device in Parkinson's disease (INTREPID): a multicentre, double-blind, randomised, sham-controlled study. *Lancet Neurol*. 2020;19:491–501. https://doi.org/10.1016/S1474-4422(20)30108-3.
78. McIntyre CC, Grill WM. Excitation of central nervous system neurons by nonuniform electric fields. *Biophys J*. 1999;76:878–888. https://doi.org/10.1016/S0006-3495(99)77251-6.
79. Mohan UR, Watrous AJ, Miller JF, et al. The effects of direct brain stimulation in humans depend on frequency, amplitude, and white-matter proximity. *Brain Stimul*. 2020;13:1183–1195. https://doi.org/10.1016/j.brs.2020.05.009.
80. Sotiropoulos SN, Steinmetz PN. Assessing the direct effects of deep brain stimulation using embedded axon models. *J Neural Eng*. 2007;4:107–119. https://doi.org/10.1088/1741-2560/4/2/011.
81. Foutz TJ, Ackermann Jr DM, Kilgore KL, McIntyre CC. Energy efficient neural stimulation: coupling circuit design and membrane biophysics. *PLoS One*. 2012;7:e51901. https://doi.org/10.1371/journal.pone.0051901.
82. Moldovan AS, Hartmann CJ, Trenado C, et al. Less is more - Pulse width dependent therapeutic window in deep brain stimulation for essential tremor. *Brain Stimul*. 2018;11:1132–1139. https://doi.org/10.1016/j.brs.2018.04.019.
83. Bouthour W, Wegrzyk J, Momjian S, et al. Short pulse width in subthalamic stimulation in Parkinson's disease: a randomized, double-blind study. *Mov Disord*. 2018;33:169–173. https://doi.org/10.1002/mds.27265.
84. McIntyre CC, Grill WM. Selective microstimulation of central nervous system neurons. *Ann Biomed Eng*. 2000;28:219–233. https://doi.org/10.1114/1.262.
85. Anderson DN, Duffley G, Vorwerk J, Dorval AD, Butson CR. Anodic stimulation misunderstood: preferential activation of fiber orientations with anodic waveforms in deep brain stimulation. *J Neural Eng*. 2019;16:016026. https://doi.org/10.1088/1741-2552/aae590.
86. BeMent SL, Ranck JB. A quantitative study of electrical stimulation of central myelinated fibers. *Exp Neurol*. 1969;24:147–170. https://doi.org/10.1016/0014-4886(69)90012-0.
87. Kirsch AD, Hassin-Baer S, Matthies C, Volkmann J, Steigerwald F. Anodic versus cathodic neurostimulation of the subthalamic nucleus: a randomized-controlled study of acute clinical effects. *Parkinsonism Relat Disord*. 2018;55:61–67. https://doi.org/10.1016/j.parkreldis.2018.05.015.
88. De Jesus S, Almeida L, Shahgholi L, et al. Square biphasic pulse deep brain stimulation for essential tremor: the BiP tremor study. *Parkinsonism Relat Disord*. 2018;46:41–46. https://doi.org/10.1016/j.parkreldis.2017.10.015.
89. Lilly JC, Hughes JR, Alvord EC, Galkin TW. Brief, noninjurious electric waveform for stimulation of the brain. *Science*. 1955;121:468–469. https://doi.org/10.1126/science.121.3144.468.
90. Merrill DR, Bikson M, Jefferys JGR. Electrical stimulation of excitable tissue: design of efficacious and safe protocols. *J Neurosci Methods*. 2005;141:171–198. https://doi.org/10.1016/j.jneumeth.2004.10.020.
91. Piallat B, Chabardès S, Devergnas A, et al. Monophasic but not biphasic pulses induce brain tissue damage during monopolar high-frequency deep brain stimulation. *Neurosurgery*. 2009;64:156–162 [discussion: 162–163]. https://dx.doi.org/10.1227/01.NEU.0000336331.88559.CF.
92. Stieger KC, Eles JR, Ludwig KA, Kozai TDY. *In vivo* microstimulation with cathodic and anodic asymmetric waveforms modulates spatiotemporal calcium dynamics in cortical neuropil and pyramidal neurons of male mice. *J Neurosci Res*. 2020;98:2072–2095. https://doi.org/10.1002/jnr.24676.
93. Hofmann L, Ebert M, Tass PA, Hauptmann C. Modified pulse shapes for effective neural stimulation. *Front Neuroeng*. 2011;4:9. https://doi.org/10.3389/fneng.2011.00009.
94. Foutz TJ, McIntyre CC. Evaluation of novel stimulus waveforms for deep brain stimulation. *J Neural Eng*. 2010;7:066008. https://doi.org/10.1088/1741-2560/7/6/066008.
95. Prodanov D, Delbeke J. Mechanical and biological interactions of implants with the brain and their impact on implant design. *Front Neurosci*. 2016;10:11. https://doi.org/10.3389/fnins.2016.00011.
96. Evers J, Lowery M. The active electrode in the living brain: the response of the brain parenchyma to chronically implanted deep brain stimulation electrodes. *Oper Neurosurg (Hagerstown)*. 2021;20:131–140. https://doi.org/10.1093/ons/opaa326.
97. Saxena T, Karumbaiah L, Gaupp EA, et al. The impact of chronic blood–brain barrier breach on intracortical electrode function. *Biomaterials*. 2013;34:4703–4713. https://doi.org/10.1016/j.biomaterials.2013.03.007.
98. Yousif N, Bayford R, Liu X. The influence of reactivity of the electrode–brain interface on the crossing electric current in therapeutic deep brain stimulation. *Neuroscience*. 2008;156:597–606. https://doi.org/10.1016/j.neuroscience.2008.07.051.
99. Ineichen C, Shepherd NR, Sürücü O. Understanding the effects and adverse reactions of deep brain stimulation: is it time for a paradigm shift toward a focus on heterogenous biophysical tissue properties instead of electrode design only? *Front Hum Neurosci*. 2018;12:468. https://doi.org/10.3389/fnhum.2018.00468.
100. Latikka J, Kuurne T, Eskola H. Conductivity of living intracranial tissues. *Phys Med Biol*. 2001;46:1611–1616. https://doi.org/10.1088/0031-9155/46/6/302.
101. Komlosh ME, Horkay F, Freidlin RZ, Nevo U, Assaf Y, Basser PJ. Detection of microscopic anisotropy in gray matter and in a novel tissue phantom using double Pulsed Gradient Spin Echo MR. *J Magn Reson*. 2007;189:38–45. https://doi.org/10.1016/j.jmr.2007.07.003.
102. Nicholson PW. Specific impedance of cerebral white matter. *Exp Neurol*. 1965;13:386–401. https://doi.org/10.1016/0014-4886(65)90126-3.
103. Howell B, McIntyre CC. Analyzing the tradeoff between electrical complexity and accuracy in patient-specific computational models of deep brain stimulation. *J Neural Eng*. 2016;13, 036023. https://doi.org/10.1088/1741-2560/13/3/036023.
104. Shimony JS, McKinstry RC, Akbudak E, et al. Quantitative diffusion-tensor anisotropy brain MR imaging: normative human data and anatomic analysis. *Radiology*. 1999;212:770–784. https://doi.org/10.1148/radiology.212.3.r99au51770.
105. Tuch DS, Wedeen VJ, Dale AM, George JS, Belliveau JW. Conductivity tensor mapping of the human brain using diffusion tensor MRI. *Proc Natl Acad Sci U S A*. 2001;98:11697–11701. https://doi.org/10.1073/pnas.171473898.
106. Grill WM. Modeling the effects of electric fields on nerve fibers: influence of tissue electrical properties. *IEEE Trans Biomed Eng*. 1999;46:918–928. https://doi.org/10.1109/10.775401.
107. Lee MB, Kim HJ, Kwon OI. Decomposition of high-frequency electrical conductivity into extracellular and intracellular compartments based on two-compartment model using low-to-high multi-b diffusion MRI. *Biomed Eng Online*. 2021;20:29. https://doi.org/10.1186/s12938-021-00869-5.
108. Yu Y, Wang X, Wang Q, Wang Q. A review of computational modeling and deep brain stimulation: applications to Parkinson's disease. *Appl Math Mech*. 2020;41:1747–1768. https://doi.org/10.1007/s10483-020-2689-9.
109. van Albada SJ, Robinson PA. Mean-field modeling of the basal ganglia-thalamocortical system. I Firing rates in healthy and parkinsonian states. *J Theor Biol*. 2009;257:642–663. https://doi.org/10.1016/j.jtbi.2008.12.018.
110. Kuramoto Y. *Chemical Oscillations, Waves, and Turbulence*19. Springer; 1984. https://doi.org/10.1007/978-3-642-69689-3.
111. Little S, Bestmann S. Computational neurostimulation for Parkinson's disease. *Prog Brain Res*. 2015;222:163–190. https://doi.org/10.1016/bs.pbr.2015.09.002.
112. Mina F, Benquet P, Pasnicu A, Biraben A, Wendling F. Modulation of epileptic activity by deep brain stimulation: a model-based study of frequency-dependent effects. *Front Comput Neurosci*. 2013;7:94. https://doi.org/10.3389/fncom.2013.00094.
113. Giannakakis E, Hutchings F, Papasavvas CA, et al. Computational modelling of the long-term effects of brain stimulation on the local and global structural connectivity of epileptic patients. *PLoS One*. 2020;15:e0221380. https://doi.org/10.1371/journal.pone.0221380.
114. Ramirez-Mahaluf JP, Roxin A, Mayberg HS, Compte A. A computational model of major depression: the role of glutamate dysfunction on cingulo-frontal network dynamics. *Cereb Cortex*. 2017;27:660–679. https://doi.org/10.1093/cercor/bhv249.
115. Albin RL, Young AB, Penney JB. The functional anatomy of basal ganglia disorders. *Trends Neurosci*. 1989;12:366–375. https://doi.org/10.1016/0166-2236(89)90074-X.
116. Montgomery EB, Baker KB. Mechanisms of deep brain stimulation and future technical developments. *Neurol Res*. 2000;22:259–266. https://doi.org/10.1080/01616412.2000.11740668.
117. Humphries MD, Gurney K. Network effects of subthalamic deep brain stimulation drive a unique mixture of responses in basal ganglia output. *Eur J Neurosci*. 2012;36:2240–2251. https://doi.org/10.1111/j.1460-9568.2012.08085.x.
118. Santaniello S, McCarthy MM, Montgomery EB, Gale JT, Kopell N, Sarma SV. Therapeutic mechanisms of high-frequency stimulation in Parkinson's disease and neural restoration via loop-based reinforcement. *Proc Natl Acad Sci USA*. 2015;112:E586–E595. https://doi.org/10.1073/pnas.1406549111.
119. Marceglia S, Guidetti M, Harmsen IE, et al. Deep brain stimulation: is it time to change gears by closing the loop? *J Neural Eng*. 2021;18(6). https://doi.org/10.1088/1741-2552/ac3267.
120. Feng XJ, Greenwald B, Rabitz H, Shea-Brown E, Kosut R. Toward closed-loop optimization of deep brain stimulation for Parkinson's disease: concepts and lessons from a computational model. *J Neural Eng*. 2007;4:L14–L21. https://doi.org/10.1088/1741-2560/4/2/L03.
121. Su F, Kumaravelu K, Wang J, Grill WM. Model-based evaluation of closed-loop deep brain stimulation controller to adapt to dynamic changes in reference signal. *Front Neurosci*. 2019;13:956. https://doi.org/10.3389/fnins.2019.00956.
122. Fleming JE, Dunn E, Lowery MM. Simulation of closed-loop deep brain stimulation control schemes for suppression of pathological beta oscillations in Parkinson's disease. *Front Neurosci*. 2020;14:166. https://doi.org/10.3389/fnins.2020.00166.
123. Zhu Y, Wang J, Li H, Liu C, Grill WM. Adaptive parameter modulation of deep brain stimulation based on improved supervisory algorithm. *Front Neurosci*. 2021;15:750806. https://doi.org/10.3389/fnins.2021.750806.
124. Popovych OV, Lysyansky B, Rosenblum M, Pikovsky A, Tass PA. Pulsatile desynchronizing delayed feedback for closed-loop deep brain stimulation. *PLoS One*. 2017;12:e0173363. https://doi.org/10.1371/journal.pone.0173363.



  

125. Popovych OV, Lysyansky B, Tass PA. Closed-loop deep brain stimulation by pulsatile delayed feedback with increased gap between pulse phases. *Sci Rep*. 2017;7:1033. https://doi.org/10.1038/s41598-017-01067-x.
126. Popovych OV, Tass PA. Multisite delayed feedback for electrical brain stimulation. *Front Physiol*. 2018;9:46. https://doi.org/10.3389/fphys.2018.00046.
127. Wong JK, Middlebrooks EH, Grewal SS, Almeida L, Hess CW, Okun MS. A comprehensive review of brain connectomics and imaging to improve deep brain stimulation outcomes. *Mov Disord*. 2020;35:741–751. https://doi.org/10.1002/mds.28045.
128. Frey J, Cagle J, Johnson KA, et al. Past, present, and future of deep brain stimulation: hardware, software, imaging, physiology and novel approaches. *Front Neurol*. 2022;13, 825178. https://doi.org/10.3389/fneur.2022.825178.
129. Akram H, Sotiropoulos SN, Jbabdi S, et al. Subthalamic deep brain stimulation sweet spots and hyperdirect cortical connectivity in Parkinson's disease. *NeuroImage*. 2017;158:332–345. https://doi.org/10.1016/j.neuroimage.2017.07.012.
130. Horn A, Reich M, Vorwerk J, et al. Connectivity Predicts deep brain stimulation outcome in Parkinson disease. *Ann Neurol*. 2017;82:67–78. https://doi.org/10.1002/ana.24974.
131. Middlebrooks EH, Tuna IS, Almeida L, et al. Structural connectivity-based segmentation of the thalamus and prediction of tremor improvement following thalamic deep brain stimulation of the ventral intermediate nucleus. *NeuroImage Clin*. 2018;20:1266–1273. https://doi.org/10.1016/j.nicl.2018.10.009.
132. Noecker AM, Choi KS, Riva-Posse P, Gross RE, Mayberg HS, McIntyre CC. StimVision software: examples and applications in subcallosal cingulate deep brain stimulation for depression. *Neuromodulation*. 2018;21:191–196. https://doi.org/10.1111/ner.12625.
133. Johnson KA, Duffley G, Anderson DN, et al. Structural connectivity predicts clinical outcomes of deep brain stimulation for Tourette syndrome. *Brain*. 2020;143:2607–2623. https://doi.org/10.1093/brain/awaa188.
134. Middlebrooks EH, Grewal SS, Stead M, Lundstrom BN, Worrell GA, Van Gompel JJ. Differences in functional connectivity profiles as a predictor of response to anterior thalamic nucleus deep brain stimulation for epilepsy: a hypothesis for the mechanism of action and a potential biomarker for outcomes. *Neurosurg Focus*. 2018;45:E7. https://doi.org/10.3171/2018.5.FOCUS18151.
135. Akram H, Miller S, Lagrata S, et al. Optimal deep brain stimulation site and target connectivity for chronic cluster headache. *Neurology*. 2017;89:2083–2091. https://doi.org/10.1212/WNL.0000000000004646.
136. Horn A, Reich MM, Ewert S, et al. Optimal deep brain stimulation sites and networks for cervical vs. generalized dystonia. *Proc Natl Acad Sci USA*. 2022;119:e2114985119. https://doi.org/10.1073/pnas.2114985119.
137. Ríos AS, Oxenford S, Neudorfer C, et al. Optimal deep brain stimulation sites and networks for stimulation of the fornix in Alzheimer's disease. *Nat Commun*. 2022;13:7707. https://doi.org/10.1038/s41467-022-34510-3.
138. Riva-Posse P, Choi KS, Holtzheimer PE, et al. A connectomic approach for subcallosal cingulate deep brain stimulation surgery: prospective targeting in treatment-resistant depression. *Mol Psychiatry*. 2018;23:843–849. https://doi.org/10.1038/mp.2017.59.
139. Barcia JA, Avecillas-Chasín JM, Nombela C, et al. Personalized striatal targets for deep brain stimulation in obsessive-compulsive disorder. *Brain Stimul*. 2019;12:724–734. https://doi.org/10.1016/j.brs.2018.12.226.
140. Coenen VA, Schlaepfer TE, Varkuti B, et al. Surgical decision making for deep brain stimulation should not be based on aggregated normative data mining. *Brain Stimul*. 2019;12:1345–1348. https://doi.org/10.1016/j.brs.2019.07.014.
141. Wang Q, Akram H, Muthuraman M, et al. Normative vs. patient-specific brain connectivity in deep brain stimulation. *NeuroImage*. 2021;224, 117307. https://doi.org/10.1016/j.neuroimage.2020.117307.
142. Miocinovic S, Noecker AM, Maks CB, Butson CR, McIntyre CC. Cicerone: stereotactic neurophysiological recording and deep brain stimulation electrode placement software system. *Acta Neurochir Suppl*. 2007;97:561–567. https://doi.org/10.1007/978-3-211-33081-4_65.
143. Frankemolle AMM, Wu J, Noecker AM, et al. Reversing cognitive-motor impairments in Parkinson's disease patients using a computational modelling approach to deep brain stimulation programming. *Brain*. 2010;133:746–761. https://doi.org/10.1093/brain/awp315.
144. Butson CR, Tamm G, Jain S, Fogal T, Krüger J. Evaluation of interactive visualization on mobile computing platforms for selection of deep brain stimulation parameters. *IEEE Trans Vis Comput Graph*. 2013;19:108–117. https://doi.org/10.1109/TVCG.2012.92.
145. Pourfar MH, Mogilner AY, Farris S, et al. Model-based deep brain stimulation programming for Parkinson's disease: the GUIDE pilot study. *Stereotact Funct Neurosurg*. 2015;93:231–239. https://doi.org/10.1159/000375172.
146. Lange F, Steigerwald F, Malzacher T, et al. Reduced programming time and strong symptom control even in chronic course through imaging-based DBS programming. *Front Neurol*. 2021;12:785529. https://doi.org/10.3389/fneur.2021.785529.
147. Waldthaler J, Bopp M, Kühn N, et al. Imaging-based programming of subthalamic nucleus deep brain stimulation in Parkinson's disease. *Brain Stimul*. 2021;14:1109–1117. https://doi.org/10.1016/j.brs.2021.07.064.
148. Reich MM, Horn A, Lange F, et al. Probabilistic mapping of the antidystonic effect of pallidal neurostimulation: a multicentre imaging study. *Brain*. 2019;142:1386–1398. https://doi.org/10.1093/brain/awz046.
149. Johansson JD, Zsigmond P. Comparison between patient-specific deep brain stimulation simulations and commercial system SureTune3. *Biomed Phys Eng Express*. 2021;7(5). https://doi.org/10.1088/2057-1976/ac0dcd.
150. Pavese N, Tai YF, Yousif N, Nandi D, Bain PG. Traditional trial and error versus neuroanatomic 3-dimensional image software-assisted deep brain stimulation programming in patients with Parkinson disease. *World Neurosurg*. 2020;134:e98–e102. https://doi.org/10.1016/j.wneu.2019.09.106.
151. Johansson JD, Alonso F, Wardell K. Patient-specific simulations of deep brain stimulation electric field with aid of in-house software ELMA. *Annu Int Conf IEEE Eng Med Biol Soc*. 2019;2019:5212–5216. https://doi.org/10.1109/EMBC.2019.8856307.
152. Naesström M, Johansson J, Hariz M, Bodlund O, Wårdell K, Blomstedt P. Distribution of electric field in patients with obsessive compulsive disorder treated with deep brain stimulation of the bed nucleus of stria terminalis. *Acta Neurochir (Wien)*. 2022;164:193–202. https://doi.org/10.1007/s00701-021-04991-0.
153. Butenko K, Bahls C, Schröder M, Köhling R, van Rienen U. OSS-DBS: open-source simulation platform for deep brain stimulation with a comprehensive automated modeling. *PLoS Comput Biol*. 2020;16:e1008023. https://doi.org/10.1371/journal.pcbi.1008023.
154. Horn A, Li N, Dembek TA, et al. Lead-DBS v2: towards a comprehensive pipeline for deep brain stimulation imaging. *NeuroImage*. 2019;184:293–316. https://doi.org/10.1016/j.neuroimage.2018.08.068.
155. Kuncel AM, Cooper SE, Grill WM. A method to estimate the spatial extent of activation in thalamic deep brain stimulation. *Clin Neurophysiol*. 2008;119:2148–2158. https://doi.org/10.1016/j.clinph.2008.02.025.
156. Mädler B, Coenen VA. Explaining clinical effects of deep brain stimulation through simplified target-specific modeling of the volume of activated tissue. *AJNR Am J Neuroradiol*. 2012;33:1072–1080. https://doi.org/10.3174/ajnr.A2906.
157. Dembek TA, Barbe MT, Åström M, et al. Probabilistic mapping of deep brain stimulation effects in essential tremor. *NeuroImage Clin*. 2017;13:164–173. https://doi.org/10.1016/j.nicl.2016.11.019.
158. Nordenström S, Petermann K, Debove I, et al. Programming of subthalamic nucleus deep brain stimulation for Parkinson's disease with sweet spot-guided parameter suggestions. *Front Hum Neurosci*. 2022;16:925283. https://doi.org/10.3389/fnhum.2022.925283.
159. Wong JK, Patel B, Middlebrooks EH, et al. Connectomic analysis of unilateral dual-lead thalamic deep brain stimulation for treatment of multiple sclerosis tremor. *Brain Commun*. 2022;4:fcac063. https://doi.org/10.1093/braincomms/fcac063.
160. Oxenford S, Roediger J, Neudorfer C, et al. Lead-OR: a multimodal platform for deep brain stimulation surgery. *eLife*. 2022;11:e72929. https://doi.org/10.7554/eLife.72929.
161. Husch A, Petersen MV, Gemmar P, Goncalves J, Hertel F. PaCER - a fully automated method for electrode trajectory and contact reconstruction in deep brain stimulation. *Neuroimage Clin*. 2017;17:80–89. https://doi.org/10.1016/j.nicl.2017.10.004.
162. Lauro PM, Vanegas-Arroyave N, Huang L, et al. DBSproc: an open source process for DBS electrode localization and tractographic analysis. *Hum Brain Mapp*. 2016;37:422–433. https://doi.org/10.1002/hbm.23039.
163. Vanegas-Arroyave N, Lauro PM, Huang L, et al. Tractography patterns of subthalamic nucleus deep brain stimulation. *Brain*. 2016;139:1200–1210. https://doi.org/10.1093/brain/aww020.
164. Duffley G, Lutz BJ, Szabo A, et al. Home health management of Parkinson disease deep brain stimulation: a randomized clinical trial. *JAMA Neurol*. 2021;78:972–981. https://doi.org/10.1001/jamaneurol.2021.1910.
165. Vorwerk J, McCann D, Krüger J, Butson CR. Interactive computation and visualization of deep brain stimulation effects using Duality. *Comput Methods Biomech Biomed Eng Imaging Vis*. 2020;8:3–14. https://doi.org/10.1080/21681163.2018.1484817.
166. Baniasadi M, Proverbio D, Gonçalves J, Hertel F, Husch A. FastField: an open-source toolbox for efficient approximation of deep brain stimulation electric fields. *NeuroImage*. 2020;223:117330. https://doi.org/10.1016/j.neuroimage.2020.117330.
167. Hirt L, Grassia F, Feuerstein J, Thompson JA, Ojemann S, Kern DS. Deep brain stimulation of the ventral intermediate nucleus of the thalamus in writer's cramp: a case report. *Tremor Other Hyperkinet Mov (N Y)*. 2021;11:46. https://doi.org/10.5334/tohm.645.
168. Petry-Schmelzer JN, Dembek TA, Steffen JK, et al. Selecting the most effective DBS contact in essential tremor patients based on individual tractography. *Brain Sci*. 2020;10:1015. https://doi.org/10.3390/brainsci10121015.
169. Fernandes Arroteia I, Husch A, Baniasadi M, Hertel F. Impressive weight gain after deep brain stimulation of nucleus accumbens in treatment-resistant bulimic anorexia nervosa. *BMJ Case Rep*. 2020;13:e239316. https://doi.org/10.1136/bcr-2020-239316.
170. Noecker AM, Frankemolle-Gilbert AM, Howell B, et al. StimVision v2: examples and applications in subthalamic deep brain stimulation for Parkinson's disease. *Neuromodulation*. 2021;24:248–258. https://doi.org/10.1111/ner.13350.
171. Shah A, Vogel D, Alonso F, et al. Stimulation maps: visualization of results of quantitative intraoperative testing for deep brain stimulation surgery. *Med Biol Eng Comput*. 2020;58:771–784. https://doi.org/10.1007/s11517-020-02130-y.
172. Anderson DN, Osting B, Vorwerk J, Dorval AD, Butson CR. Optimized programming algorithm for cylindrical and directional deep brain stimulation electrodes. *J Neural Eng*. 2018;15:026005. https://doi.org/10.1088/1741-2552/aaa14b.




  

## COMMENTS

This is a very nice primer for those new to how engineering/computational principles are positioned to help navigate and optimize DBS therapy. An inescapable tenet of this paper, and indeed the field, is that even biology and neuroscience must obey the laws of physics. From a true pioneer in the field, Dr McIntyre, the paper provides a much needed tutorial on fundamental principles of neural stimulation and patient specific imaging, giving rise to computational tractable predictions to volumes of tissue that are activated during DBS. The contribution includes an "over-the-horizon" view as to how computational models and new science such as connectomics will influence the future of DBS.

Joseph Pancrazio, PhD
*Dallas, TX, USA*

***

Computational modeling has a long history in deep brain stimulation and in other areas of neuromodulation. This review provides a valuable introduction to the biophysics of deep brain stimulation, how parameter selection influences this, and how computational modeling of these physical phenomena can be used to inform our understanding of deep brain stimulation and optimizing stimulation parameters. These techniques are becoming increasingly important to progress in neuromodulation, and understanding their strengths and limitations is essential to accurately evaluate emerging evidence and comprehend their role in clinical decision making. This work provides a useful overview of the major considerations in modeling of deep brain stimulation for a clinical audience who may need to engage with this area of research.

Conor Keogh, MB, BCh, MSc, MRCS
*Oxford, United Kingdom*



  